

2-p
mix

NTIS
HC #6.25

(NASA-CR-130288) FLOX/MMH ROCKET ENGINE N73-15814
ASSEMBLIES Final Report, March 1972
(Rocketdyne) 81 p HC \$6.25 CSCL 21H
Unclas
G3/28 52038



Rocketdyne
North American Rockwell

41 p8



Rocketdyne
North American Rockwell

6633 Canoga Avenue,
Canoga Park, California 91304

NTIS
HC #6,25

R-8960

FINAL REPORT
FLOX/MMH ROCKET ENGINE ASSEMBLIES

MARCH 1972

Contract No. 953206

Prepared For
National Aeronautics and Space Administration

R. M. Knight
Project Engineer
Rocketdyne
A Division of North American Rockwell Corporation
Canoga Park, California

Publication Date: October 1972

This work was performed for the Jet Propulsion
Laboratory, California Institute of Technology
sponsored by the National Aeronautics and Space
Administration under Contract NAS7-100.

Details of illustrations in
this document may be better
studied on microfiche

FOREWORD

This report was prepared in compliance with NASA Contract 953206, entitled "FLOX/MMH Rocket Engine Assemblies." Mr. T. Price, Jet Propulsion Laboratory, was the NASA Project Manager. Rocketdyne Program Manager was Mr. F. E. Campagna, with technical approach and guidance supplied by Dr. R. N. Gurnitz. The Project Engineer was Mr. R. M. Knight.

ABSTRACT

A 6-month program was conducted to fabricate, acceptance test, and deliver to JPL two FLOX/MMH rocket engine assemblies. Acceptance testing consisted of injector cold flows and 15-second-duration hot firings with the engine assemblies. An additional objective of the program was to determine the feasibility of utilizing FLOX/MMH thrust chamber components with the F_2/N_2H_4 propellant combination. Feasibility studies consisted of analysis, cold flow, and comparative F_2/N_2H_4 -FLOX/MMH calorimeter hot fire testing, followed by a 500-second duration F_2/N_2H_4 demonstration test.

ACKNOWLEDGMENT

Significant contributions to the conduct of the program were made by the following personnel:

W. Buck, C.A. Labertew, B. L. McFarland, E. J. Ostrowski, G. N. Storey, and D. E. Zwald.

CONTENTS

Foreword	iii
Abstract	iii
Acknowledgement.	v
Introduction and Summary.	1
Hardware Description	3
Like-Douplet Injector	3
Ablative Thrust Chamber	6
Copper Calorimeter Chamber	15
Facilities	19
Propulsion Research Area (PRA)	19
Results and Discussion	25
Injector Cold Flow	25
Thermal and Erosion Analyses	34
Calorimeter Hot Firings	37
FLOX(70)/MMH	37
F ₂ /N ₂ H ₄	46
F ₂ /N ₂ H ₄ Demonstration Firing.	51
Hot-Fire Acceptance Tests.	58
Concluding Remarks	71
References	73

ILLUSTRATIONS

1.	Orifice Pattern of the Self-Impinging Doublet Injector	4
2.	C* Efficiency vs. Chamber Length for the Self-Impinging Doublet Injector	5
3.	Schematic of Like-Doublet Injector	7
4.	FLOX/MMH R.E.A. Injector	8
5.	Schematic of Ablative Thrust Chamber	9
6.	FLOX/MMH R.E.A. Ablative Thrust Chamber	10
7.	Throat Insert Modification	12
8.	Ablative Engine Instrumentation	13
9.	Ablative Chamber Thermocouple Locations	14
10.	Copper Calorimeter Thrust Chamber	16
11.	Calorimeter Engine Instrumentation	17
12.	Photographs Depicting the Cold-Flow Distribution Measurement Apparatus	21
13.	FLOX-F ₂ Flow System and Instrumentation Schematic	22
14.	MMH-N ₂ H ₄ Flow System and Instrumentation Schematic	23
15.	R.E.A. Injector Flow Calibration	26
16.	Cold Flow Mixing Efficiency	28
17.	C* vs. Mixture Ratio for FLOX(70).MMH and F ₂ /N ₂ H ₄	30
18.	Mass and Mixture Ratio Profiles for Injector No. 1 (Flox/MMH M.R. = 1.98)	31
19.	Cold-Flow Collection Matrix	32
20.	Core and Wall Mixture Ratios vs. Overall Mixture Ratio for Injector No. 1	33
21.	Bartz Film Coefficient and Heat Flux for FLOX(70)/MMH and F ₂ /N ₂ H ₄	35
22.	Predicted Throat Erosion Rates	36
23.	Copper Calorimeter Chamber Installation	38
24.	Measured Wall Static Pressure Profile for FLOX(70)/MMH	41
25.	C* and I _{s vac} Efficiency for FLOX(70)/MMH	43
26.	FLOX(70)/MMH Chamber Wall Heat Flux for Run Nos. 1 and 2	44
27.	FLOX(70)/MMH Chamber Wall Heat Flux for Run Nos. 3 and 4	45

28.	Throat Heat Flux and Film Coefficient for FLOX(70)/MMH	47
29.	Chamber Wall Pressure Profile for F_2/N_2H_4	49
30.	F_2/N_2H_4 Chamber Wall Heat Transfer	50
31.	Injector End View of Ablative Chamber After 500-Second Firing with F_2/N_2H_4	52
32.	Nozzle End View of Ablative Chamber After 500-Second Firing with F_2/N_2H_4	53
33.	Self-Impinging Doublet Injector After 500-Second Firing with F_2/N_2H_4 (Prior to Cleaning)	54
34.	Sectioned View of Ablative Thrust Chamber After 500-Second F_2/N_2H_4 Firing	55
35.	Composite Ablative Thrust Chamber After a 1000-Second-Duration Firing with FLOX(70)/MMH (Program NAS7-304)	57
36.	Ablative Chamber Wall Temperature at Positions 1, 5, and 9	59
37.	Ablative Chamber Wall Temperature at Positions 2, 6, and 10.	60
38.	Ablative Chamber Wall Temperature at Positions 3, 7, and 11.	61
39.	Ablative Chamber Wall Temperature at Positions 4, 8, and 12.	62
40.	FLOX/MMH R.E.A. Installation	63
41.	Chamber Pressure and Thrust for the Two Acceptance Tests.	65
42.	R.E.A. Like-Doublet Injectors After 15-Second Acceptance Tests.	67
43.	R.E.A. Graphite Throat Insert After 15-Second Acceptance Test	68
44.	R.E.A. Ablative Liner After 15-Second Acceptance Test	69
45.	Throat Temperature Response Measured During the Two Acceptance Tests	70

TABLES

1. Cold Flow Results	27
2. Hot-Fire Data Summary	39
3. Ablative Chamber Measurements	56

INTRODUCTION AND SUMMARY

This report summarizes the results of a program to fabricate and acceptance test two FLOX/MMH engine assemblies for the Jet Propulsion Laboratory. These engines, designed during a previous program (Ref. 1), are to be incorporated into a space-storable propulsion module for overall system performance evaluation by JPL.

An additional objective of the program was to determine the feasibility of using the FLOX/MMH hardware with the F_2/N_2H_4 propellant combination. Analytical, cold flow, and comparative F_2/N_2H_4 - FLOX/MMH calorimeter hot fire studies were made to determine basic feasibility, followed by a 500-second-duration F_2/N_2H_4 demonstration test.

The acceptance test procedure consisted of injector mass and mixture ratio distribution cold flows, and a 15-second-duration hot fire test with each assembly. The two engines exhibited excellent structural integrity and c^* efficiency, the latter being above the minimum required level of 6000 ft/sec.

The analytical and experimental F_2/N_2H_4 feasibility studies indicated that this propellant combination would perform in an acceptable manner using the FLOX/MMH thrust chamber components. This was verified in a successful 500-second duration test.

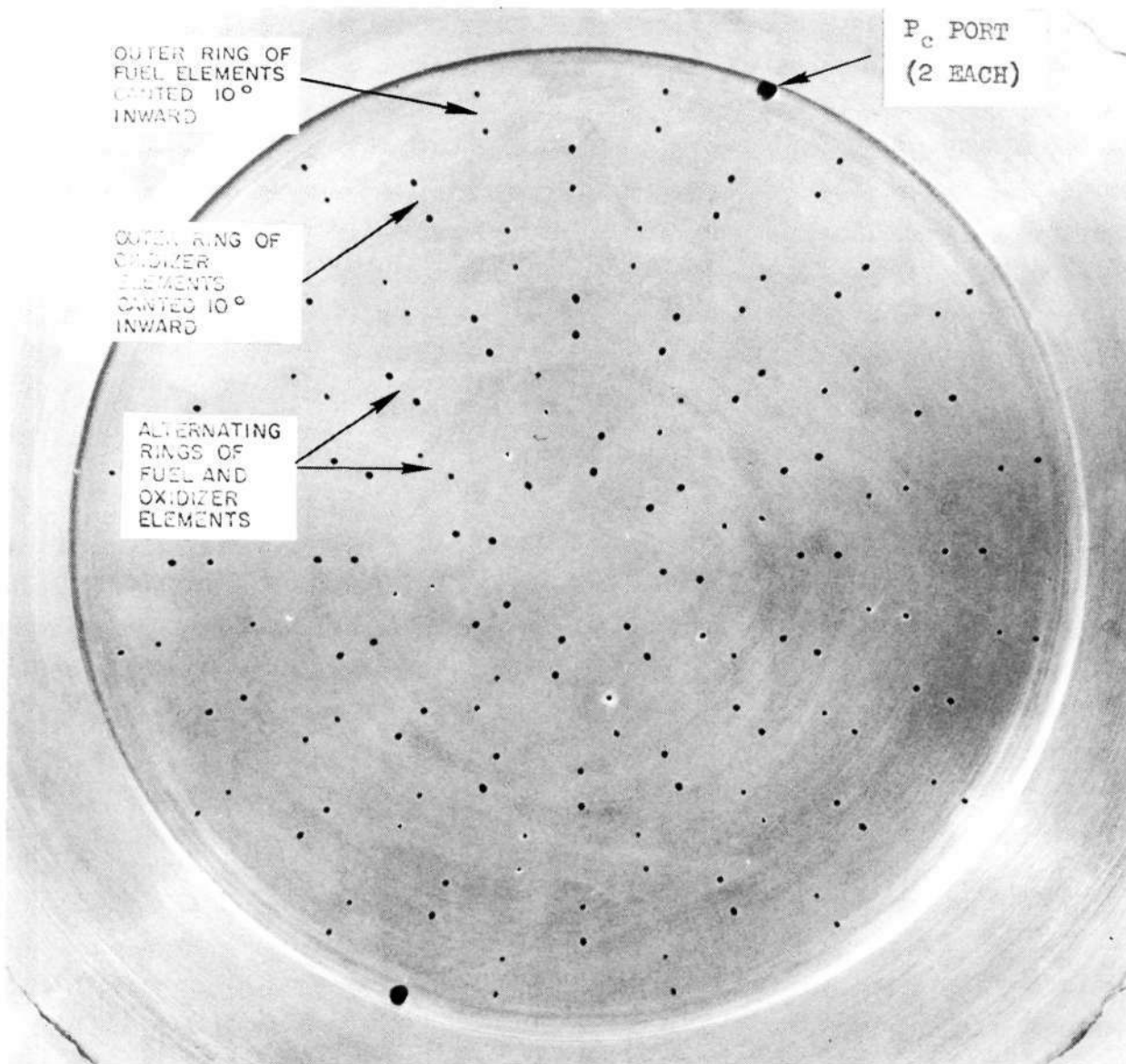
HARDWARE DESCRIPTION

This section presents a description of the individual components which comprise the FLOX/MMH Rocket Engine Assembly and the calorimeter chamber used in the F_2/N_2H_4 feasibility studies. In addition, a description of test instrumentation is included.

LIKE-DOUBLET INJECTOR

The self-impinging doublet injector, designed specifically for ablative applications, incorporates 80 elements arranged in a radial pattern of alternating fuel and oxidizer rings (Fig. 1). The outermost ring consists of fuel elements (pairs of 0.020-inch-diameter fuel orificies) canted 10 degrees inward to avoid direct impingement of the propellant fans on the chamber walls. The next ring toward the center consists of oxidizer elements (pairs of 0.025-inch-diameter oxidizer orificies) also canted 10 degrees inward to prevent direct wall impingement. The total oxidizer flow area is 0.0388 sq. in., while that for the fuel is 0.0241 sq. in.; the ratio of oxidizer to fuel orifice diameters is 1.25. The orifice pattern shown in Fig. 1 was designed to produce a gradient in mixture ratio across the face of the injector, from fuel-rich conditions (mixture ratios of 1.0 or less) at the outer periphery to the nominal design mixture ratio (2.0) in the central portion of the spray. With the FLOX(70)/MMH propellants, a mixture ratio reduction near the chamber wall results in a minimal amount of water vapor and unconsumed oxidizer in this region, thus minimizing char and erosion rates in the ablative chamber.

The like-doublet injector was found to exhibit high performance ($\eta_{c^*} > 95$ percent) in reasonably short combustion chambers. The variation of c^* efficiency with chamber length, obtained during Task II of the NAS7-304 program (Ref. 1), is presented in Fig. 2. The c^* efficiency for the FLOX/MMH ablative chambers ($L = 10.3$ inches) is approximately 96 percent. It should be noted that this performance level could be increased by minor adjustment of relative spray fan orientation but was considered beyond the scope of the present program.



5AA34-10/26/71-S2A

Figure 1. Orifice Pattern of the Self-Impinging Doublet Injector

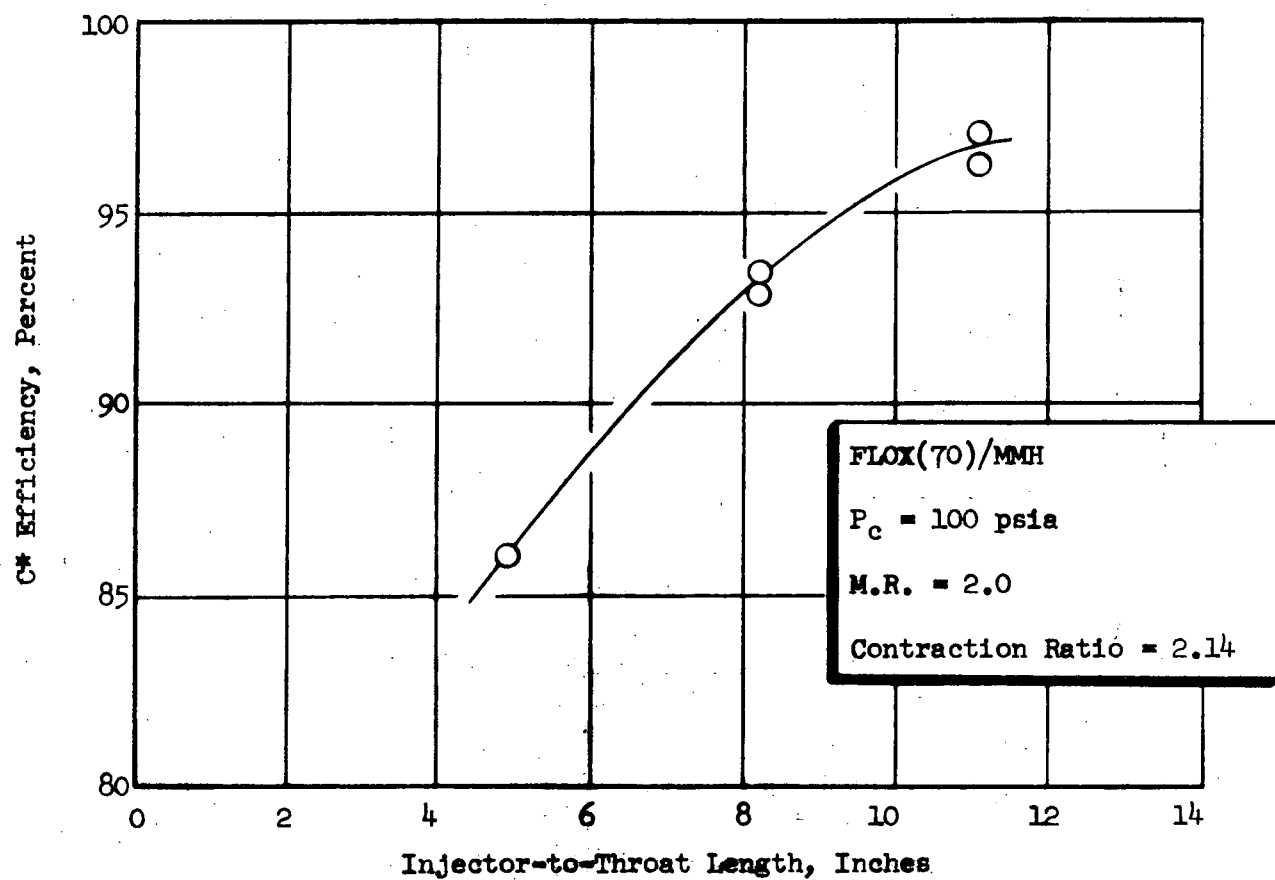


Figure 2. C^* Efficiency vs. Chamber Length for the Self-Impinging Doublet Injector (Ref. 1)

A schematic of the injector is shown in Fig. 3. The all-welded assembly, shown in Fig. 4, consists of a nickel body, nickel oxidizer dome, and a stainless steel fuel manifold. The use of the nickel material was found to result in excellent durability in the Ref. 1 program during which one injector was hot-fired for more than 4500 seconds in continuous (1000-second maximum), pulse restart, and cyclic restart operation at sea-level and at altitude with chamber pressures ranging from 100 to 180 psia.

The body, the oxidizer dome, and the manifold are circumferentially aligned in such a way that the orifice feeders are offset with respect to the propellant inlets. Conventional machining and welding techniques were utilized in the fabrication of the two injectors; however, the injector orifices were formed by an EDM process. This process has been found to produce burr-free orifice entrances, a condition which reduces the probability of jet misimpingement.

Instrumentation ports were incorporated for measurement of fuel manifold temperature and pressure, oxidizer manifold temperature and pressure, and chamber pressure at two locations on the injector face.

ABLATIVE THRUST CHAMBER

The ablative thrust chamber is shown in Fig. 5 and 6. In terms of overall dimensions, this design is essentially the same as that employed in the 1000-second-duration tests conducted during the NAS7-304 program. The chamber assembly consists of an 0.8-inch-thick carbon cloth/phenolic resin liner with a Refrasil cloth/phenolic resin overwrap. A 0.4-inch counterbore is provided at the aft end of the liner for insertion of the ATJ graphite throat insert. A porous carbon washer is incorporated downstream of the throat to allow for thermal expansion of the ablative and graphite materials.

The ablative chamber is enclosed in a three-piece steel case assembly. The outer shell is fabricated of carbon steel with welded flanges at both ends. The nozzle-end retainer plate (also carbon steel) is designed to restrain both the ablative liners and the graphite throat. This design ensures positive retention of the throat insert.

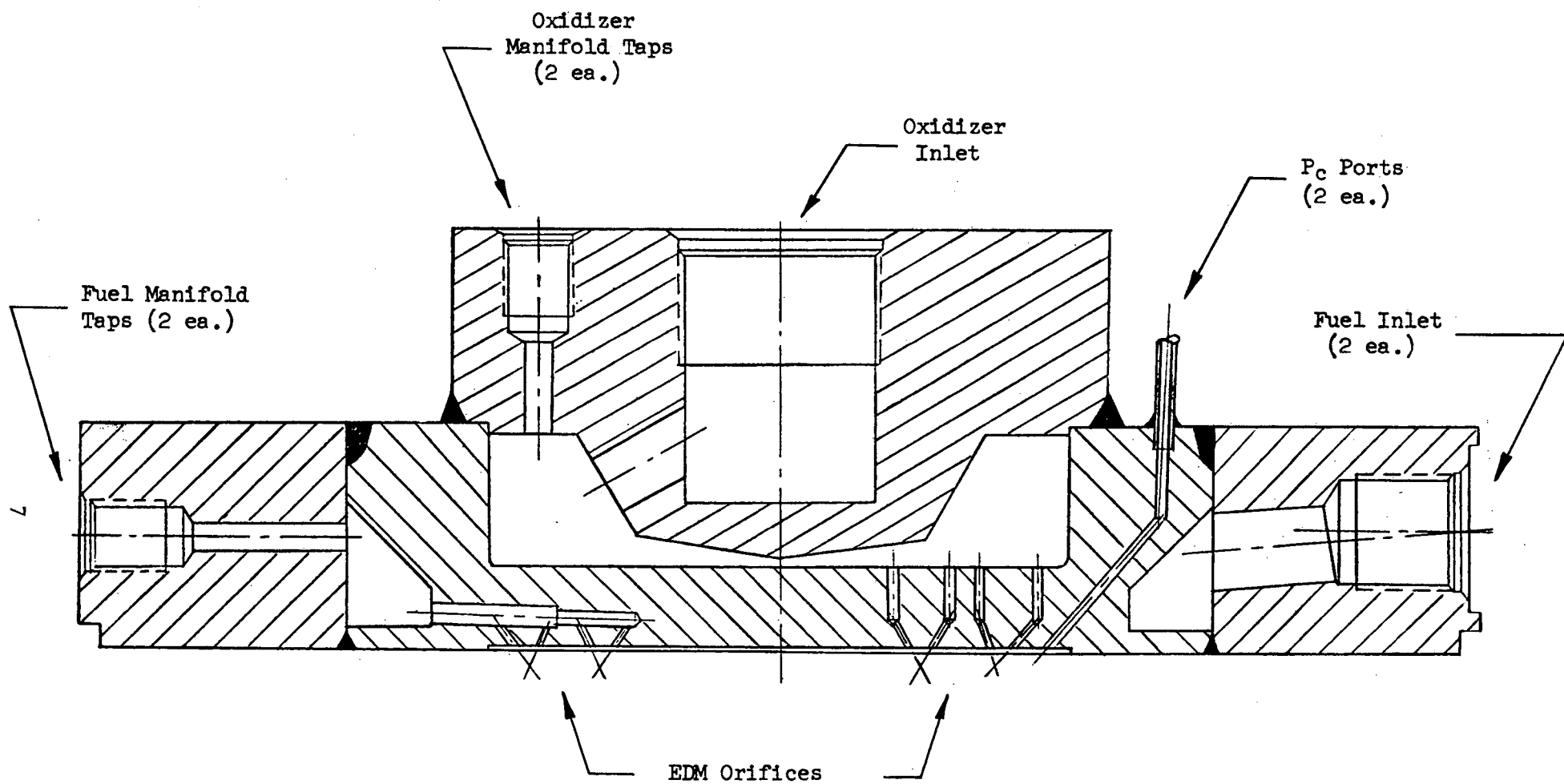
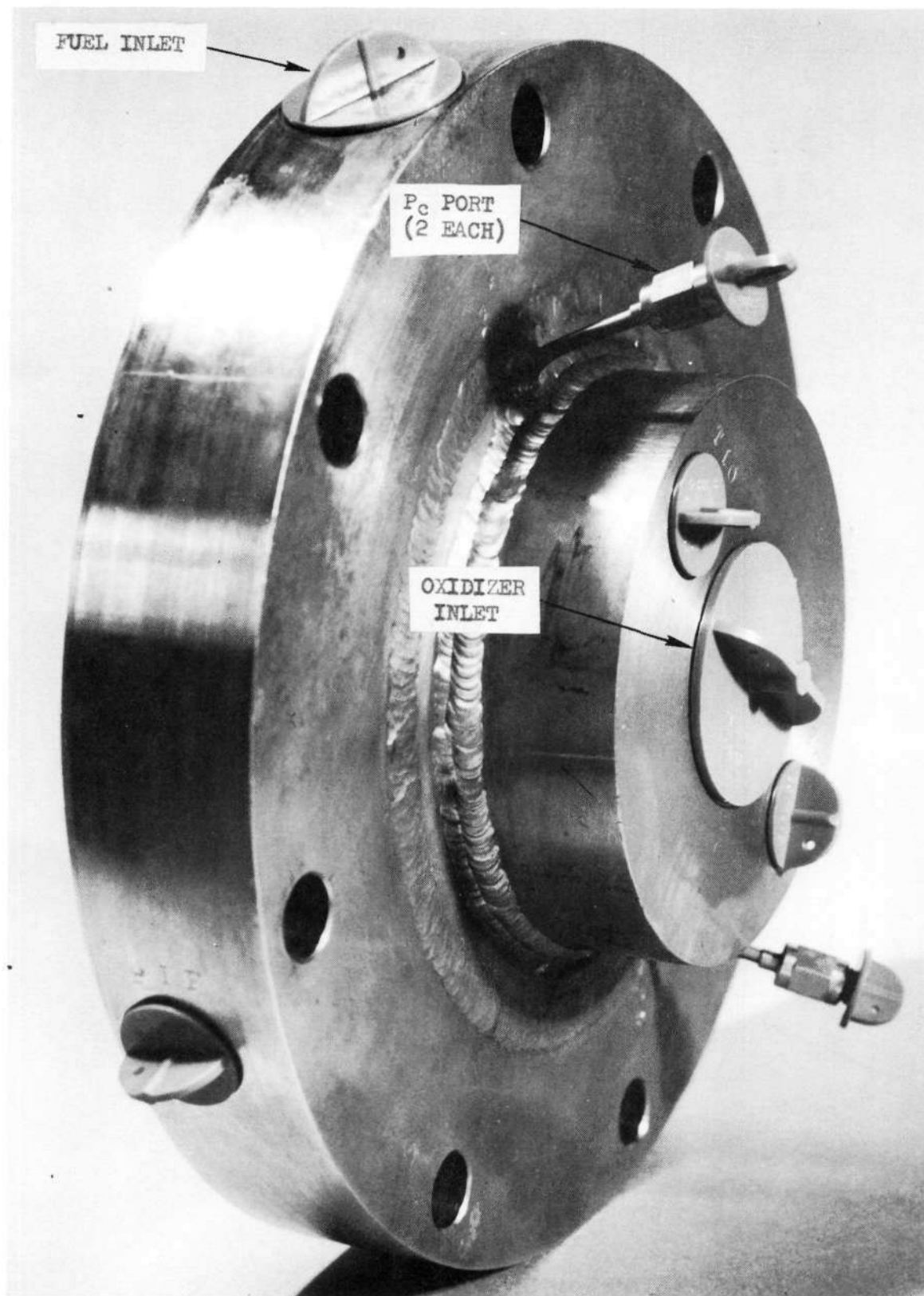


Figure 3. Schematic of Like-Doublet Injector



5AA34-10/26/71-S2B

Figure 4. FLOX/MMH R.E.A. Injector

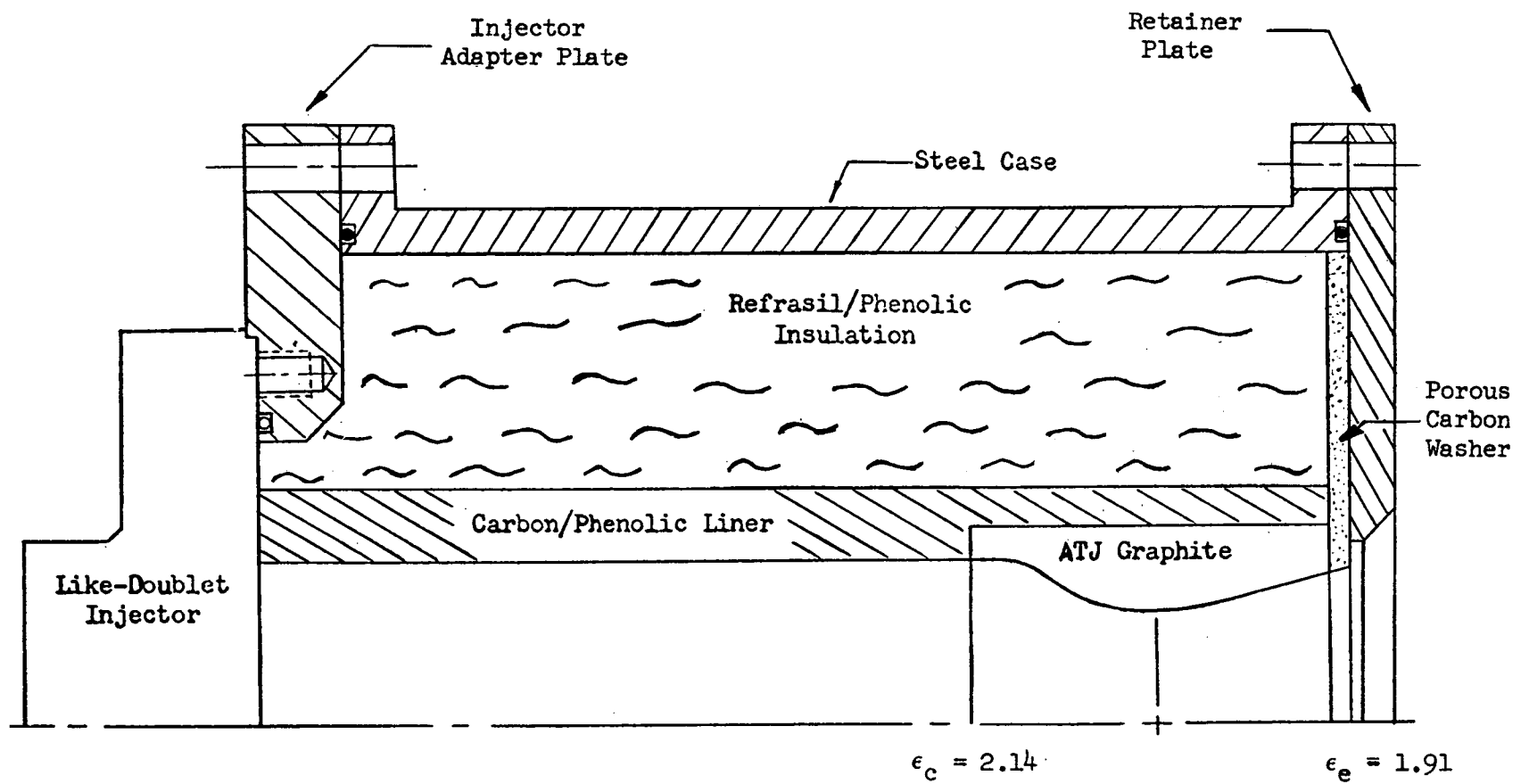
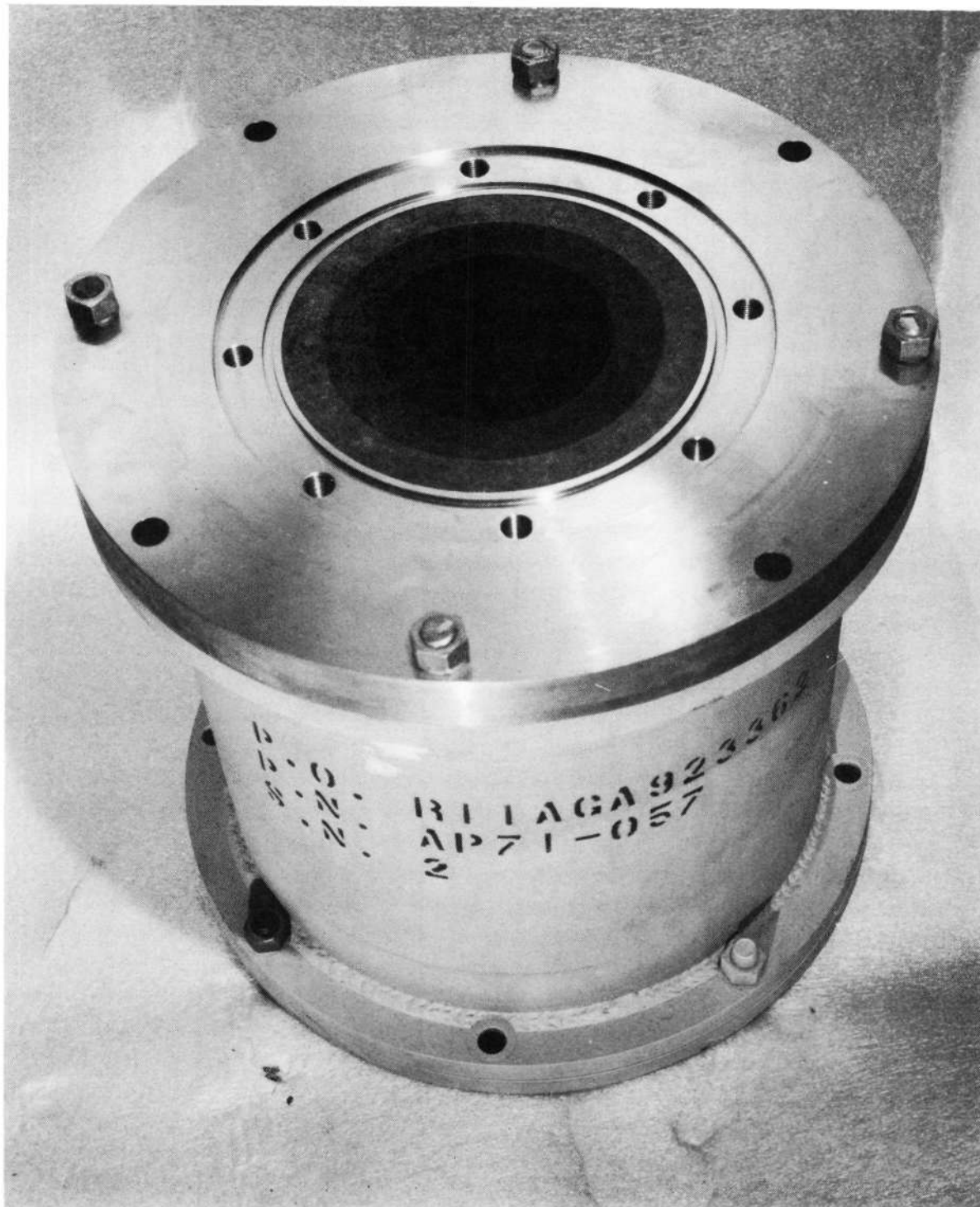


Figure 5. Schematic of Ablative Thrust Chamber



5AA44-11/4/71-S2A

Figure 6. FLOX/MMH R.E.A. Ablative Thrust Chamber

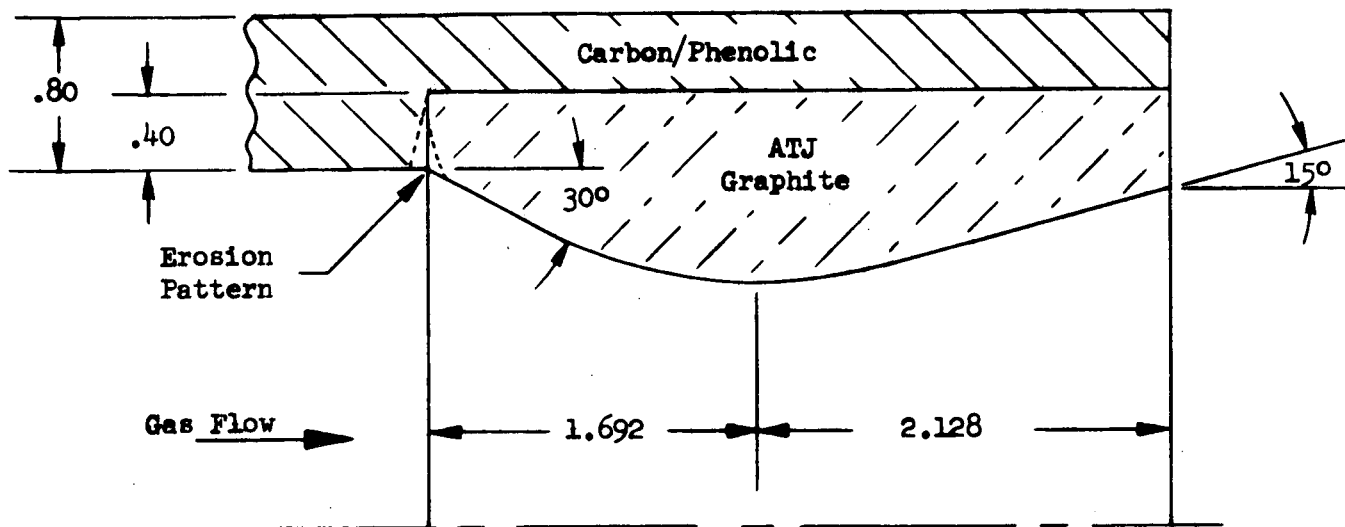
The stainless steel injector adapter plate incorporates a positioning ring for accurate radial alignment of the injector. Elastomeric o-rings are used for the injector-chamber seal and the two chamber case flange seals.

From a thermal (char depth) standpoint the chamber design is conservative. The 3.5-inch ablative wall thickness was originally based on an estimated char depth for an 1800-sec (1/2 hour) continuous firing. From past experience on the NAS7-304 program, the char depth after 1000 seconds (including heat soakback) is about 2 inches, leaving 1.5 inches of virgin Refrasil material.

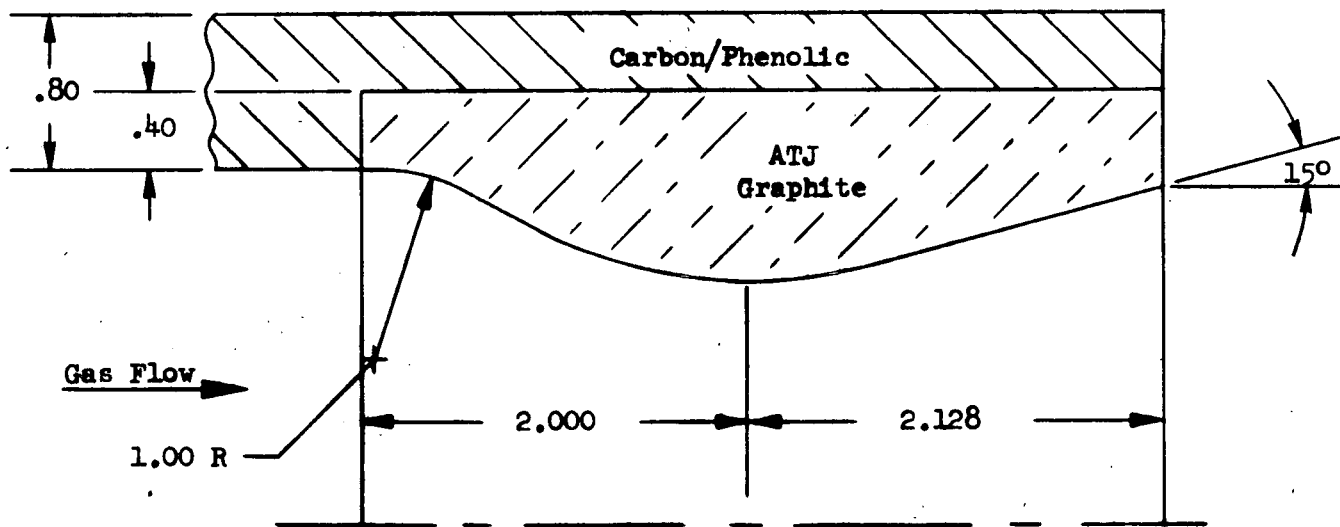
During the course of the NAS7-304 program (Task VI, Ref. 2), it was observed that char depth was a function of the carbon cloth laminate orientation. At small laminate angles (referenced to centerline) char rate was minimized. The carbon/phenolic liners have been constructed and evaluated with laminate orientation as low as 6 degrees. However, tape-wrapping at this low angle is difficult and expensive. Since overall char depth was not critical for this engine design, a 30-degree angle was used. Previous testing had shown that the overall structural integrity of the chamber is not compromised by the larger wrap angle.

One additional modification was made and is illustrated in Fig. 7. In the original design, the transition from the carbon/phenolic liner to the graphite throat insert was located at the start of nozzle convergence. As a result, undersirable local erosion was encountered at this point. The modified transition geometry was designed to reduce this phenomenon by placing the joint slightly upstream of the start of convergence. In addition, a 1-inch radius was incorporated at the start of convergence to avoid the stress problems associated with a sharp corner. The overall thickness and downstream design parameters remained the same.

Ablative engine instrumentation is shown in Fig. 8. There were 12 tungsten/rhenium thermocouples embedded in the ablative material at locations shown in Fig. 9. Chamber pressure was measured at the two injector face ports only, with a third transducer added for redundancy.

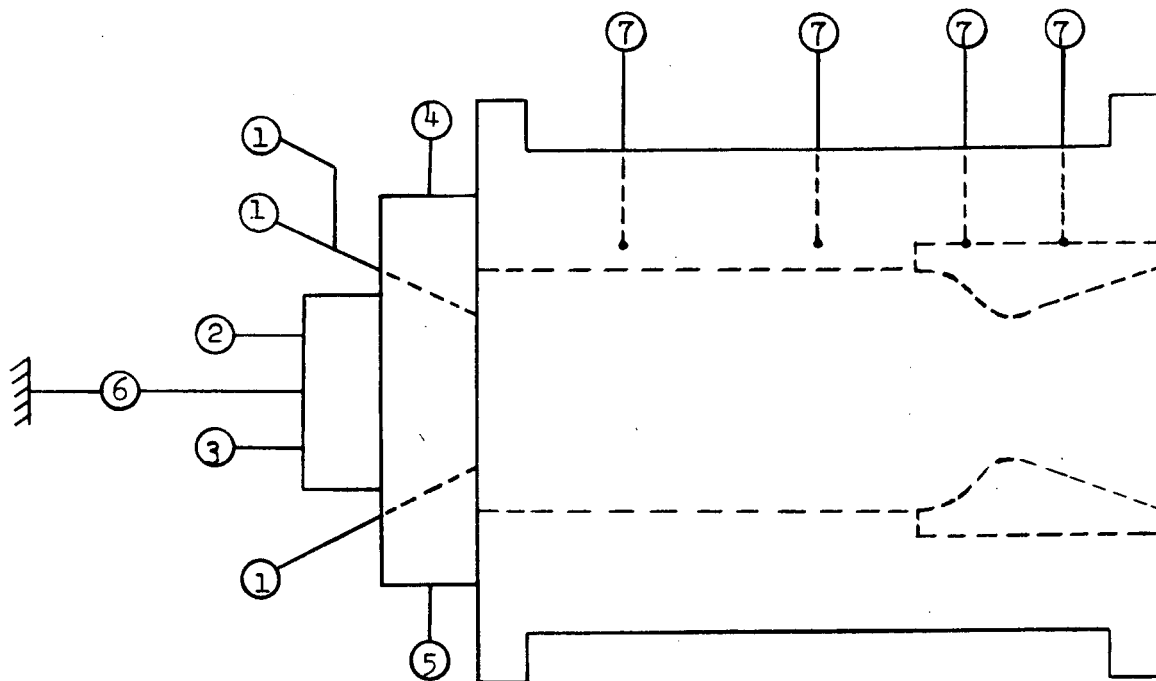


a. Original Design



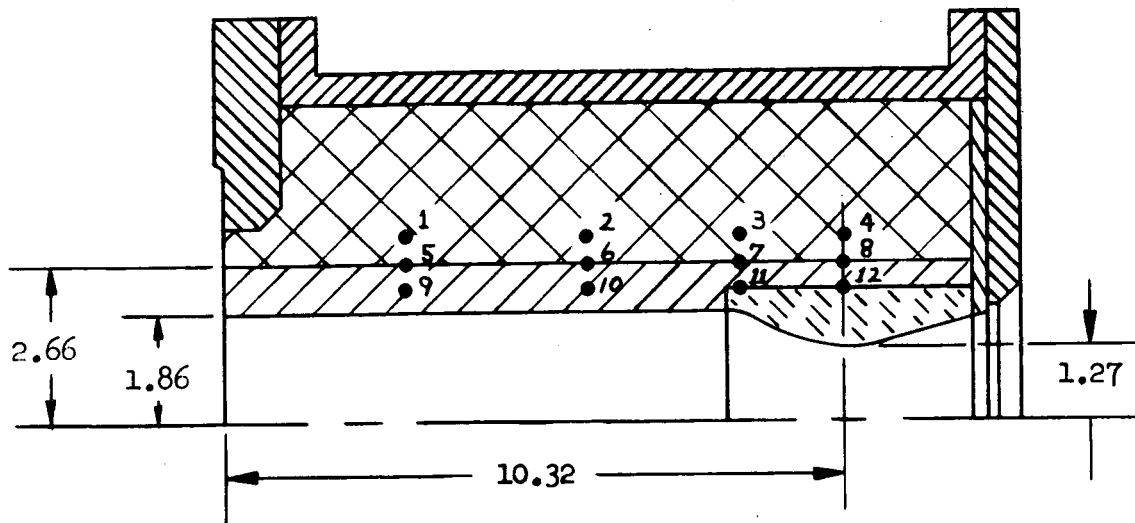
b. Modified Design

Figure 7. Throat Insert Modification



- ① Chamber Pressure (3 each)
- ② Oxidizer Manifold Pressure
- ③ Oxidizer Manifold Temperature
- ④ Fuel Manifold Pressure
- ⑤ Fuel Manifold Temperature
- ⑥ Thrust
- ⑦ Ablative Wall Temperature
(4 each at 0°, 120°, 240°)

Figure 8. Ablative Engine Instrumentation



Number	Thermocouple Location		
	Axial	Radial	Circumferential
1	3.00 in.	3.06 in.	0 Degrees
2	6.00	"	"
3	8.57	"	"
4	10.32	"	"
5	3.00	2.66	120
6	6.00	"	"
7	8.57	"	"
8	10.32	"	"
9	3.00	2.26	240
10	6.00	"	"
11	8.57	"	"
12	10.32	"	"

Figure 9. Ablative Chamber Thermocouple Locations

COPPER CALORIMETER CHAMBER

During the comparative F_2/N_2H_4 - FLOX/MMH calorimeter studies, an uncooled copper thrust chamber was used for measurement of combustion performance and heat transfer. The chamber and nozzle sections, illustrated in Fig. 10, have wall thicknesses of 0.25 and 0.375 inch, respectively, and are lined with a thin gold plating to prevent reaction of the hydrazine fuels with the copper. Each section has three rows of thermally isolated heat transfer segments located 120 degrees apart. Chromel/alumel thermocouples are peened into the outer surface of each segment.

The R.E.A. injectors were mated to the cylindrical chamber with a 0.39-inch carbon steel adapter plate. This gave a chamber length (injector face to throat) of 10.32 inches, the same length as in the ablative chambers.

A schematic of the calorimeter chamber instrumentation is presented in Fig. 11. Wall temperature was measured at 27 locations to provide both axial and circumferential heat flux variations. Chamber pressure was measured at 5 axial locations in addition to the two located at the injector face. A high frequency transducer (Photocon) was flush-mounted in the chamber for monitoring combustion stability.

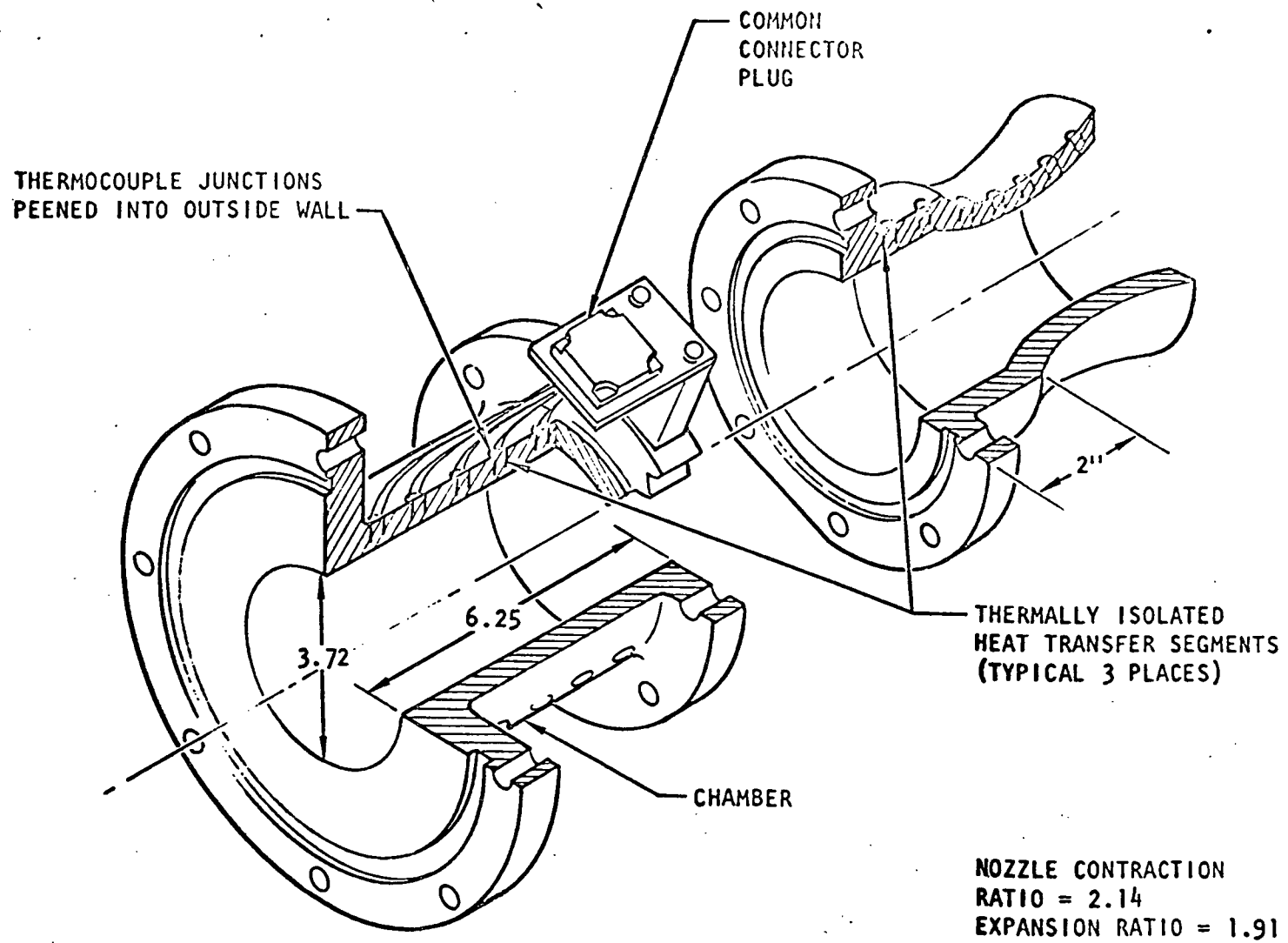


Figure 10. Copper Calorimeter Thrust Chamber

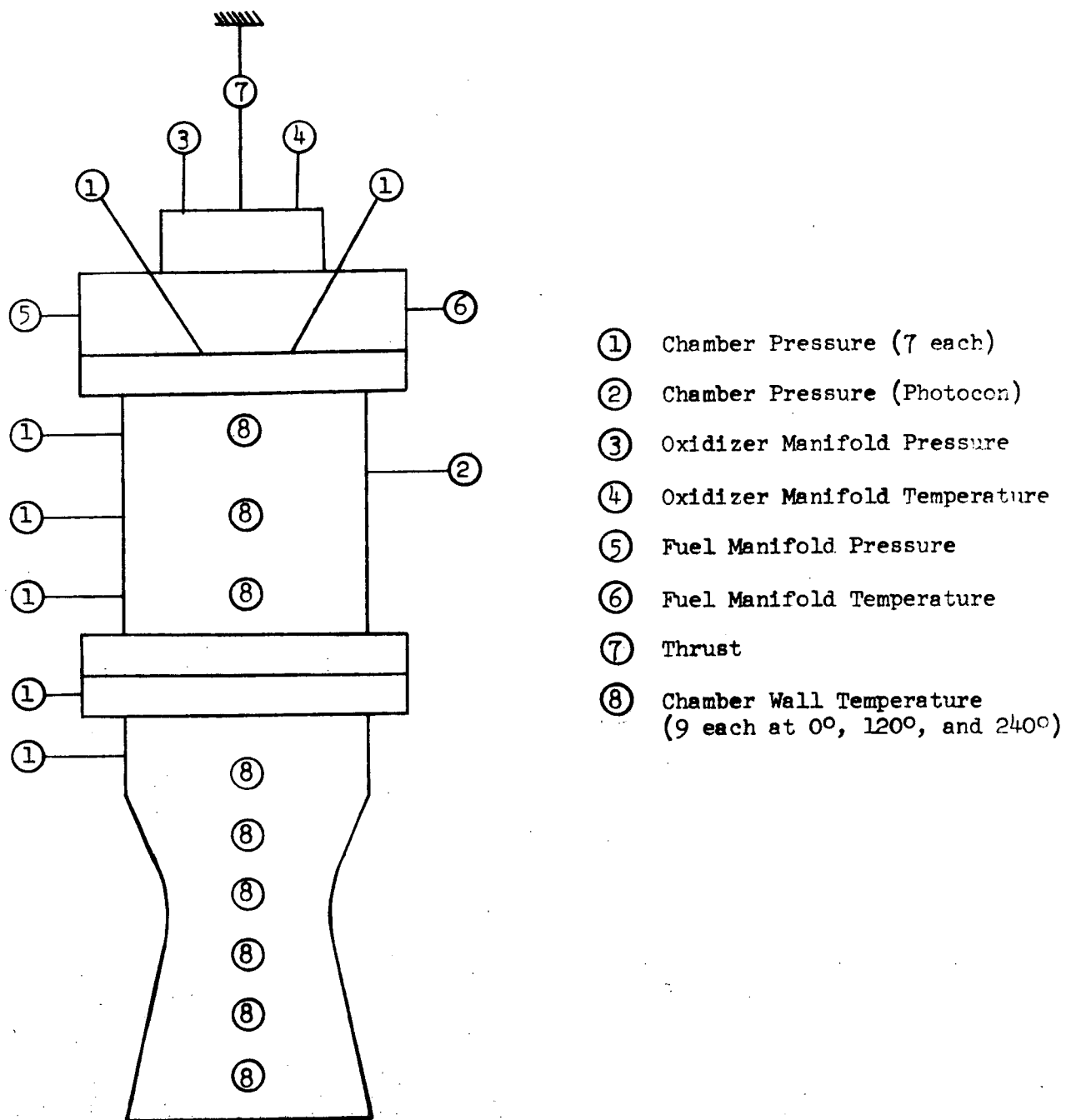


Figure 11. Calorimeter Engine Instrumentation

FACILITIES

PROPULSION RESEARCH AREA (PRA)

Experimental program activities were conducted at the Propulsion Research Area (PRA) at the Rocketdyne Santa Susana Field Laboratory (SSFL). The specialized function of this facility is to accommodate experimental research associated with advanced engine technology and propellant evaluation. Highly specialized service groups provide support in the areas of instrumentation, data acquisition, valve and component servicing, and guidance in safety precautions.

The PRA is composed of four firing pits and an auxiliary service installation. A centrally located blockhouse permits direct observation of the engine firings. The propellant supply system is distributed in the pit area to conform to the nature of propellant usage, with a complement of twenty 40-gallon-capacity tanks at a minimum of 2000-psi pressure rating. Each stand is normally serviced from a pair of low-volume propellant tanks to reduce possible safety hazards.

Primary control of firings is maintained through the use of a solid-state timer. Sequencing of operational events is normally maintained to within ± 1 millisecond tolerance although more precise control is also available if required. In addition, preselected parameters may be monitored during a firing by means of solid-state control comparator units. Automatic cutoff of the test firing can be accomplished if any of the critical parameters being monitored falls above or below a selected signal level.

Cold-Flow System

Part of the experimental facility at PRA is devoted to analyzing the mass and mixture ratio distribution produced by the injectors. Tanks of trichloroethylene and dionized water deliver the simulants at pressures up to 950 psi. Injectors are mounted over a collection matrix composed of 841 (29 x 29) 1/4-inch-square tubes which empty into 600-milliliter containers. A pneumatically operated

shutter is used to deflect the injector flow until steady-state conditions are reached, at which time the shutter opens for a timed interval. The volumes of the immiscible fluids are recorded across the matrix and input to a digital computer program which calculates mixing indices and plots various selected parameter distributions. Photographs of this facility are shown in Fig. 12.

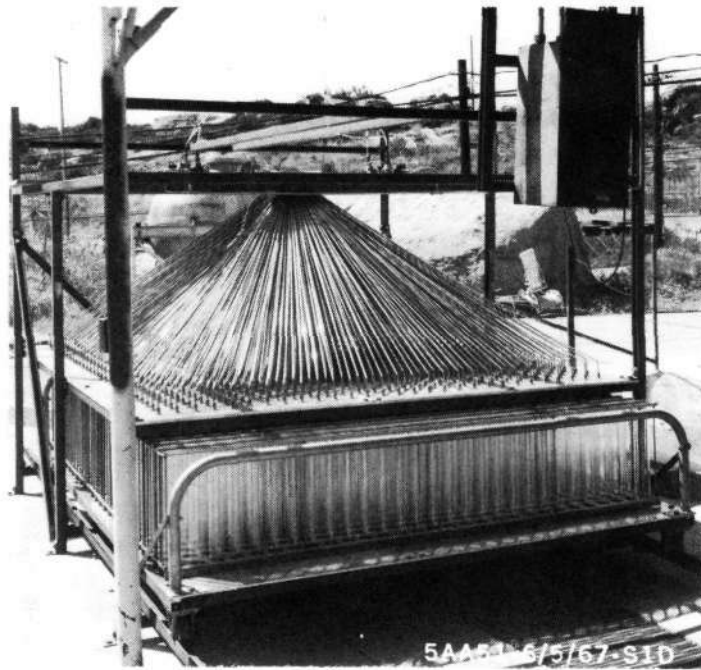
Hot-Fire Facility

The hot-fire acceptance tests were conducted on Yoke stand in the Propulsion Research Area. This test stand is fully equipped to store and deliver a wide variety of space-storable propellants. The fluorinated oxidizer system, shown in Fig. 13, contains both storage vessels and run tanks for delivery of FLOX and F_2 . The facility is limited in FLOX/MMH run durations to 800 seconds at the 1000-pound thrust level and F_2/N_2H_4 durations to 600 seconds. The longer durations are not limited by tank capacity, but by safety requirements which limit F_2 storage in any vessel to 1000 pounds.

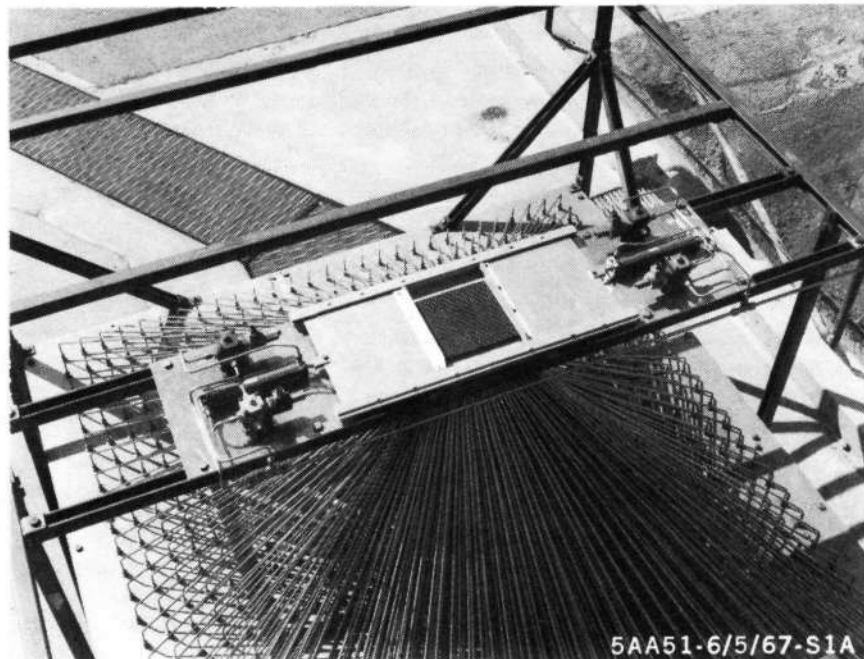
The hydrazine fuels, both neat compounds and blends, are stored in a centrally located "tank farm" area. These high pressure vessels are also utilized as run tanks, as illustrated in Fig. 14.

Temperature control of the cryogenic oxidizers is maintained by the use of liquid nitrogen jacketed storage tanks and line sections. The hydrazine fuels are stored and delivered at ambient temperature. Helium is used in the oxidizer system for tank pressurization, with GN_2 as the fuel pressurant and purge gas for both fuel and oxidizer injector purges. Liquid nitrogen is also delivered to the injector through the oxidizer purge system for injector temperature conditioning prior to engine start.

System pressures are measured with bonded strain gauge transducers; flowrates (volumetric) are measured with redundant turbine flowmeters; oxidizer and fuel line temperatures are sensed by platinum resistance temperature bulbs and iron-constant thermocouples, respectively, each located near the corresponding flowmeters.



Overall View of Collector



Shutter Arrangement

Figure 12. Photographs Depicting the Cold-Flow Distribution Measurement Apparatus

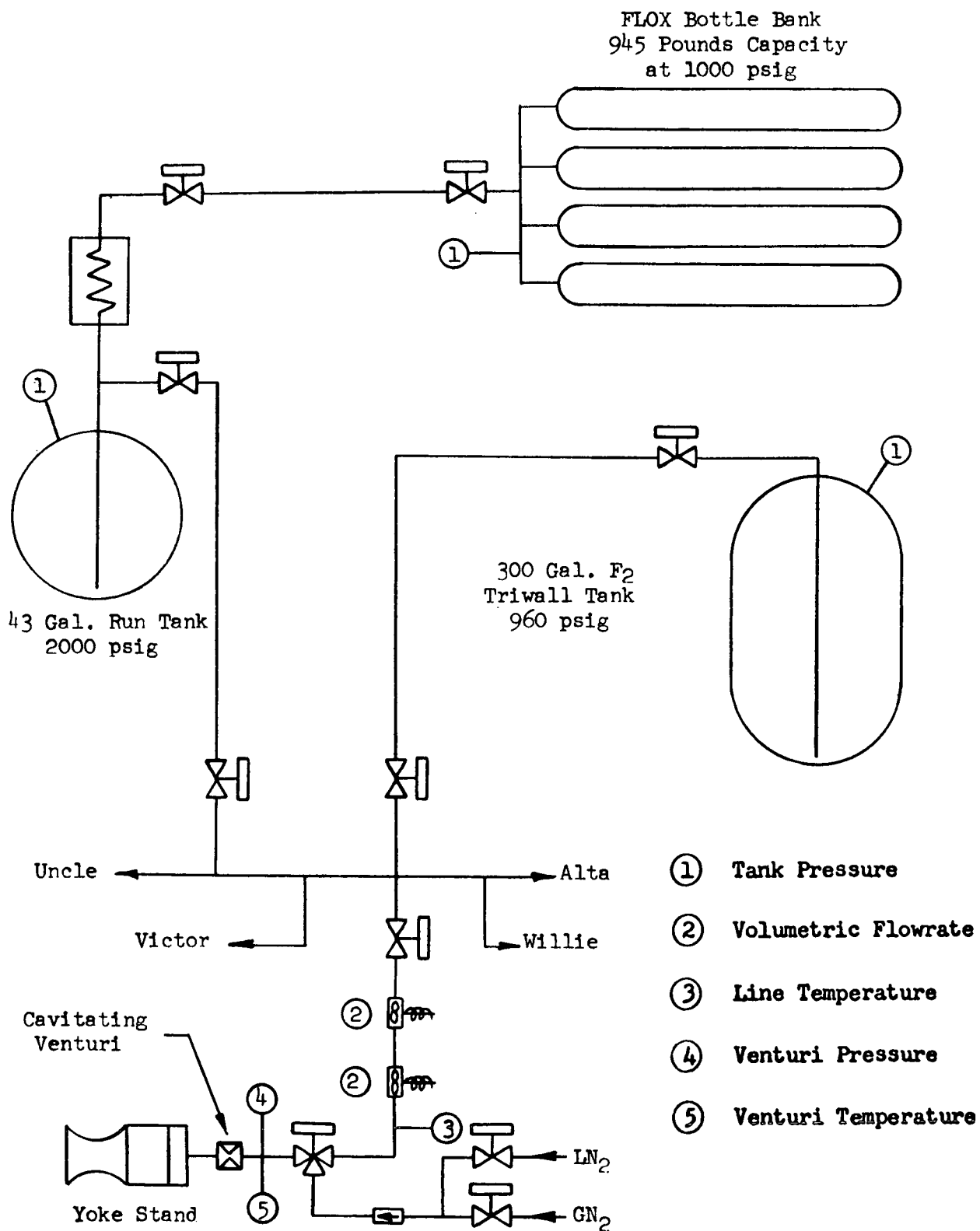


Figure 13. FLOX-F₂ Flow System and Instrumentation Schematic

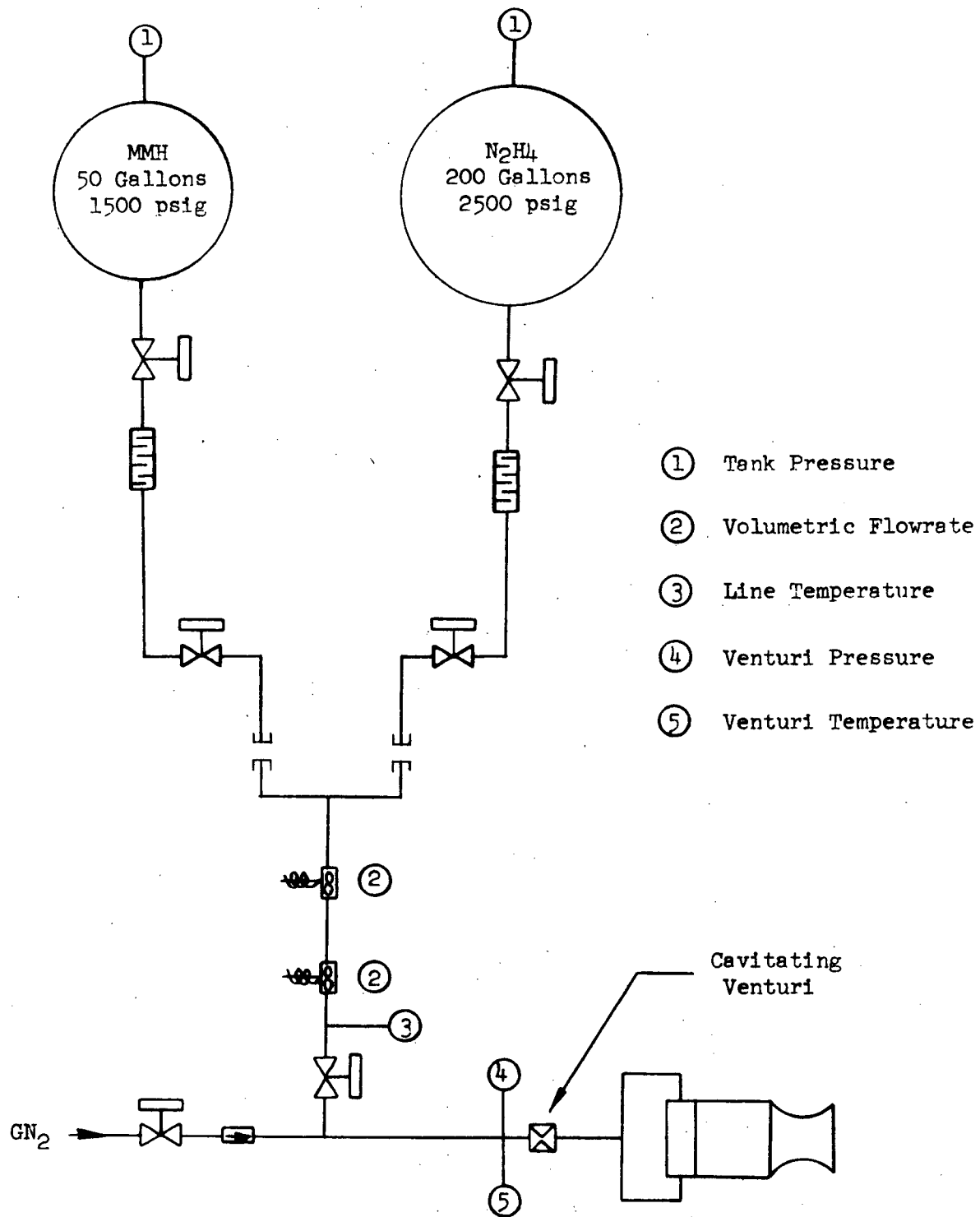


Figure 14. MMH-N₂H₄ Flow System and Instrumentation Schematic

Data Acquisition Systems

Data acquisition systems used in the PRA fall into three categories: (1) quick look data for on-site run monitoring, (2) high response rate instrumentation recording systems, and (3) low response rate-high accuracy data recording systems.

Category 1 consists of Dynalogs, strip charts, Datarite oscillographs, and closed-circuit TV cameras with playback. Category 2 includes high paper speed oscillographic recordings and an Ampex wide-band Model FR-1400, 7-channel tape recorder. Category 3 is a Beckman Model 210 digital data acquisition system. This equipment will handle a maximum of 5625 data samples per second. Sixty-six channels are available, with a resolution of one part in 4000.

RESULTS AND DISCUSSION

INJECTOR COLD FLOW

As part of the acceptance test procedure, both REA injectors were subjected to hydraulic calibration and mass and mixture ratio distribution flows. The latter tests were designed to simulate both FLOX(70)/MMH and F_2/N_2H_4 to enable a comparison of cold-flow mixing efficiency ($\eta_{c^*, mix}$) for the two propellant systems. Both studies were made using trichloroethylene and water as oxidizer and fuel simulants.

Hydraulic Calibration

The two injectors were flowed over a wide range to determine injector pressure drop as a function of flowrate. Discharge coefficients, calculated from the data of Fig. 15 at 100 psi ΔP , were 0.69 and 0.70 for injectors 1 and 2 on the oxidizer size, and 0.61 and 0.64 on the fuel side for injectors 1 and 2, respectively. The C_D values for the "EDM" orifices are more consistent between injectors than the coefficients obtained in previous work with "twist drilled" injectors manufactured from 200 series nickel.

Mass and Mixture Ratio Distribution

Three flows were conducted with each injector utilizing the previously described cold flow test facility. Injector to collector distance was maintained constant at 3.25 inches. Simulant flowrates were determined on the basis of matching the FLOX(70)/MMH momentum ratio over a mixture ratio range from 1.5 to 3.0. These tests also served to simulate F_2/N_2H_4 over about the same range since the propellant density ratios for these two combinations is about the same.

The results of these studies are presented in Table 1 and Fig. 16. From the standpoint of the mixing index defined by Rupe (E_M) (Ref. 3) and the stream tube c^* efficiency ($\eta_{c^*, mix}$), both injectors are practically identical.

PROPELLANT SIMULANTS

OXIDIZER: TRICHLOROETHYLENE

FUEL: WATER

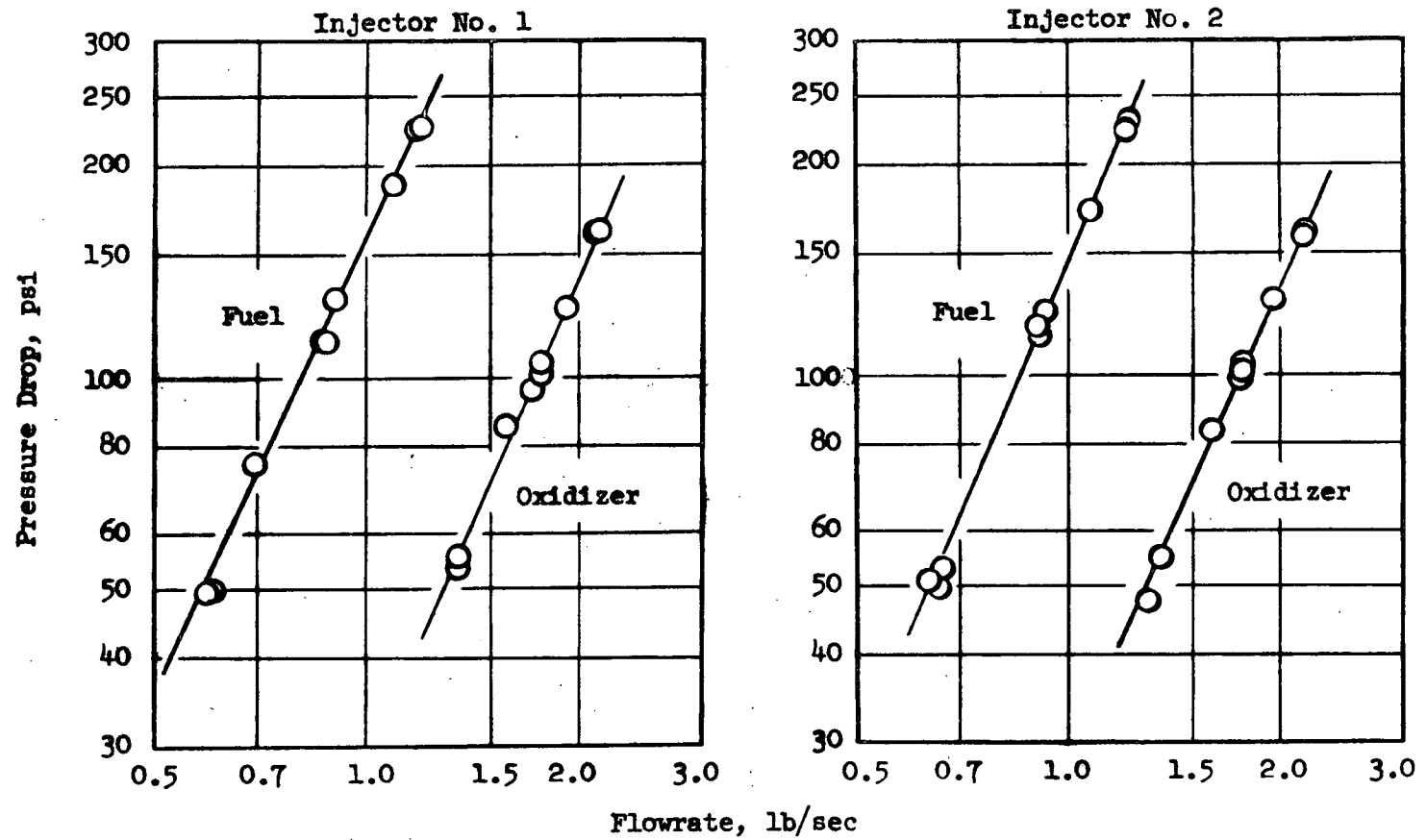


Figure 15. R.E.A. Injector Flow Calibration

TABLE 1. COLD FLOW RESULTS

Inj. No.	Run No.	Cold Flow		FLOX(70)/MMH		F_2/N_2H_4	
		Mixture Ratio	E_m	Mixture Ratio	$\eta_{c*,mix}$	Mixture Ratio	$\eta_{c*,mix}$
1	1	1.45	74.9	1.51	96.2	1.48	97.0
	2	1.90	79.7	1.98	96.9	1.94	96.8
	3	2.78	82.2	2.90	96.9	2.84	94.5
2	4	1.45	75.5	1.55	95.4	1.52	96.2
	5	1.90	79.3	1.98	96.7	1.94	96.6
	6	2.94	82.2	3.07	96.9	3.00	94.3

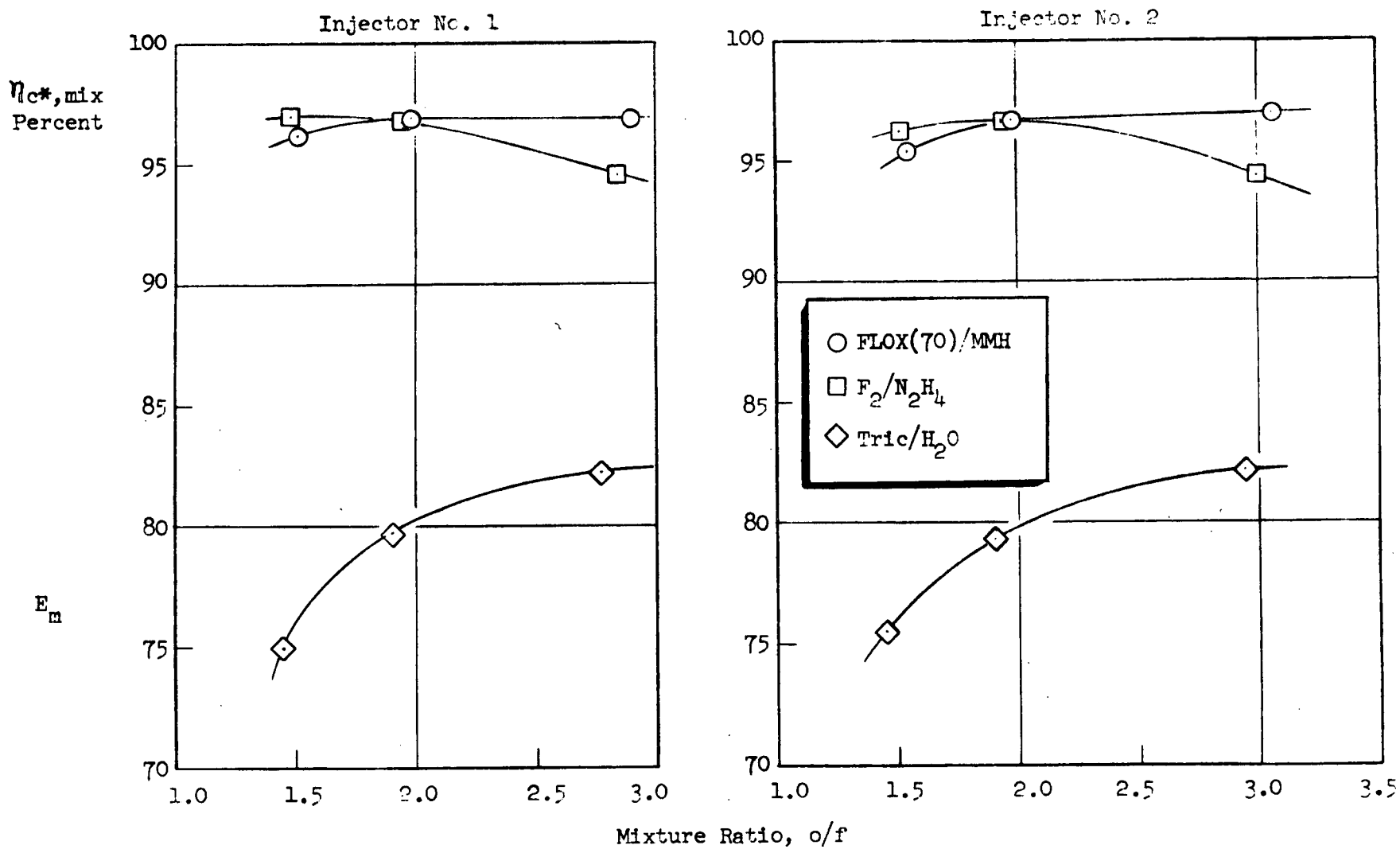


Figure 16. Cold Flow Mixing Efficiency

The curves of $\eta_{c^*,mix}$ for the two propellants show slightly different trends with mixture ratio. The decay in theoretical performance at mixture ratios greater than optimum is much greater for F_2/N_2H_4 than for FLOX(70)/MMH, as shown in Fig. 17. As a result, any locally high mixture ratio regions will produce greater performance losses with F_2/N_2H_4 . However, within the range of 1.5 to 2.0, which is the area of interest, the predicted c^* efficiencies are about the same for the two propellant combinations.

An additional objective of the cold flow studies was to determine the mixture ratio in the near-wall region as a function of overall injected mixture ratio. These data, in conjunction with the heat transfer and throat erosion analysis, were required to further define the operating point for the F_2/N_2H_4 demonstration firing. Generally, low wall mixture ratios are particularly important in ablative chamber applications since moderate gas temperatures and low levels of corrosive species are necessary to limit wall erosion rates.

Isometric plots of the mass and mixture ratio profiles are shown in Fig. 18 for an overall mixture ratio of 2.0. It is evident that the mixture ratio in the outer region is lower than in the central part of the spray. However, the extremely low mass flux in the outer area makes it difficult to accurately determine the wall mixture ratio from a plot of this type. Another method frequently used is to divide the spray field into two zones and to use the mixture ratio in the outer zone (which encompassed about 25 percent of the mass flow) in the heat transfer and erosion analyses. This was done as illustrated in Fig. 19.

The results are shown in Fig. 20 in which both the core and wall mixture ratios are plotted as a function of the overall mixture ratio. At an overall level of 2.0, the wall mixture ratio is 1.1, which is the same value experienced with twist drilled injectors during the NAS7-304 program (Ref. 1).

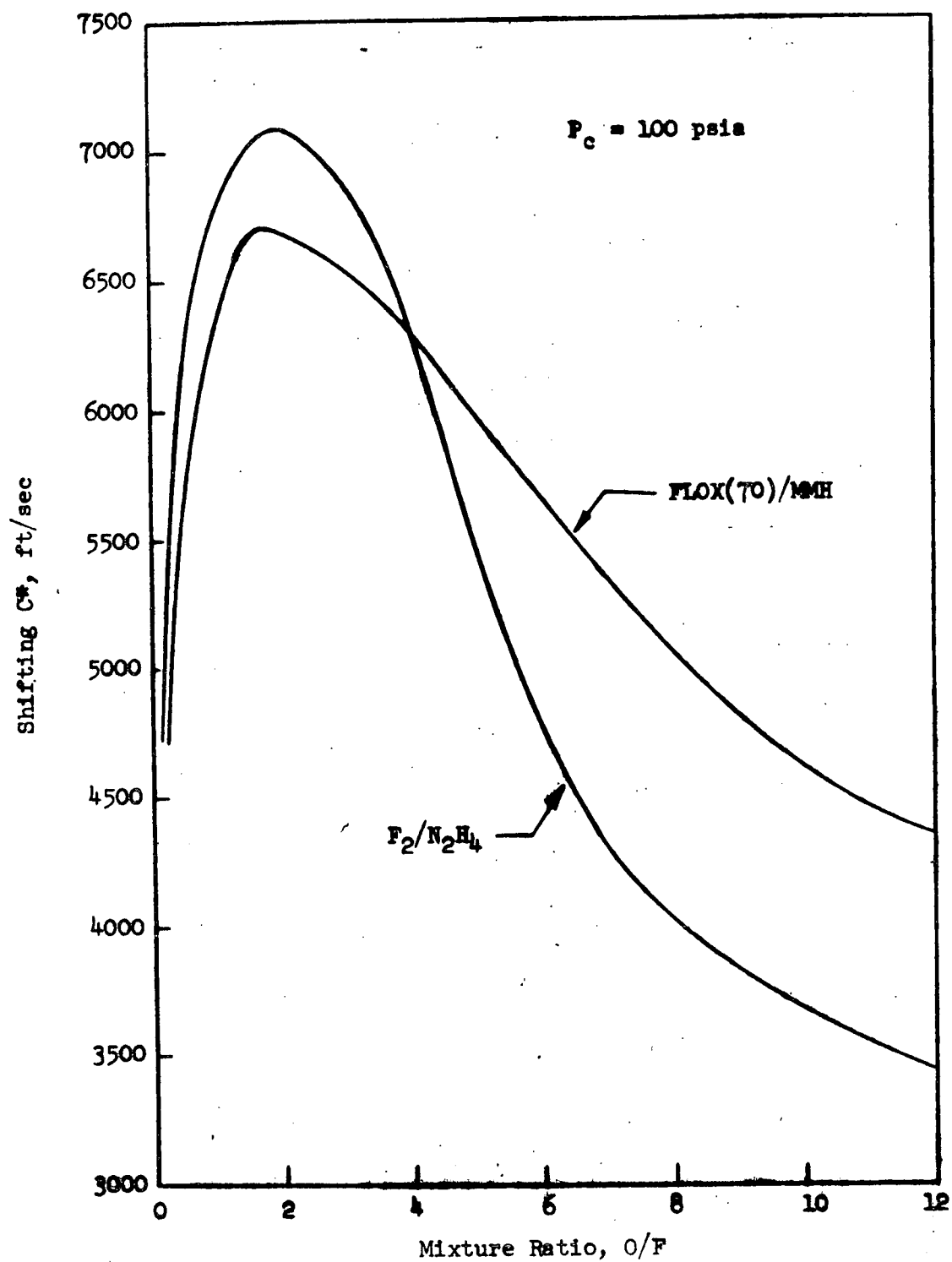


Figure 17. C^* vs. Mixture Ratio for FLOX(70)/MMH and F_2/N_2H_4

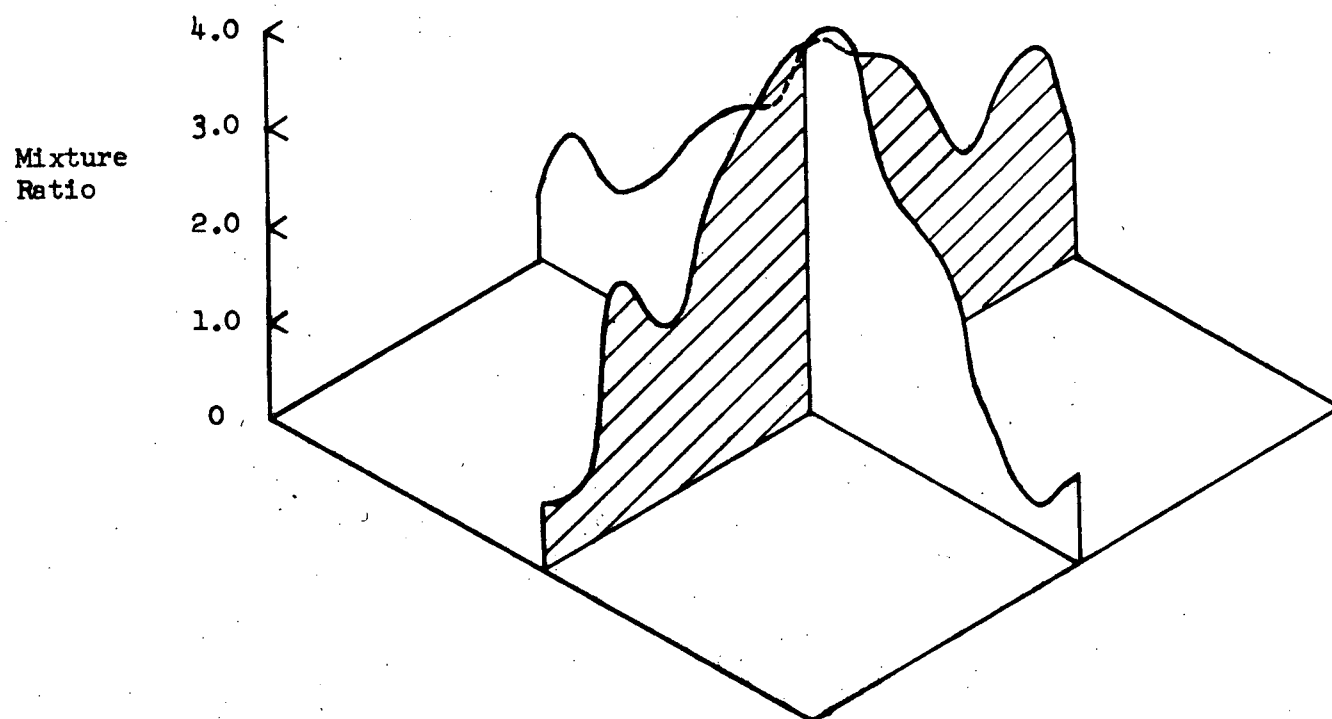
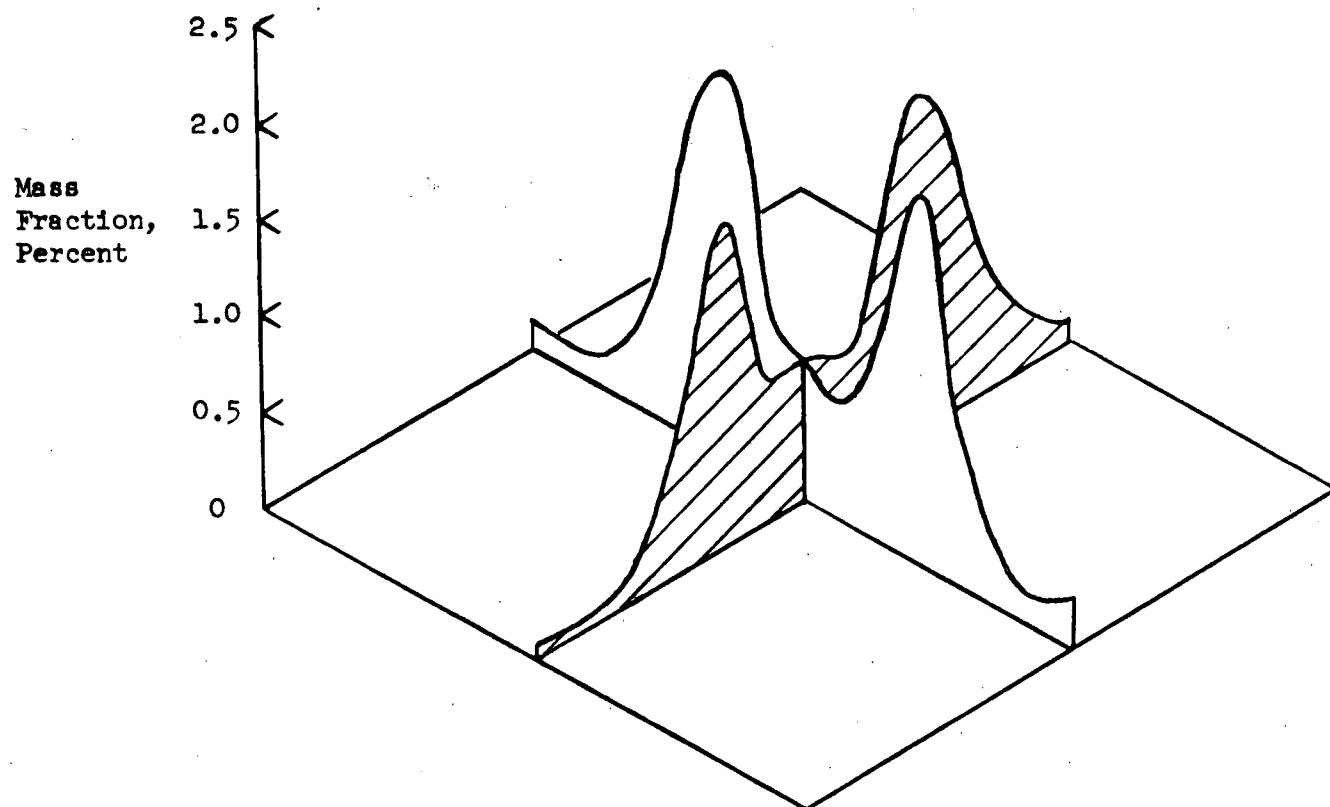


Figure 18. Mass and Mixture Ratio Profiles for Injector No. 1
(FLOX/MMH M.R. = 1.98)

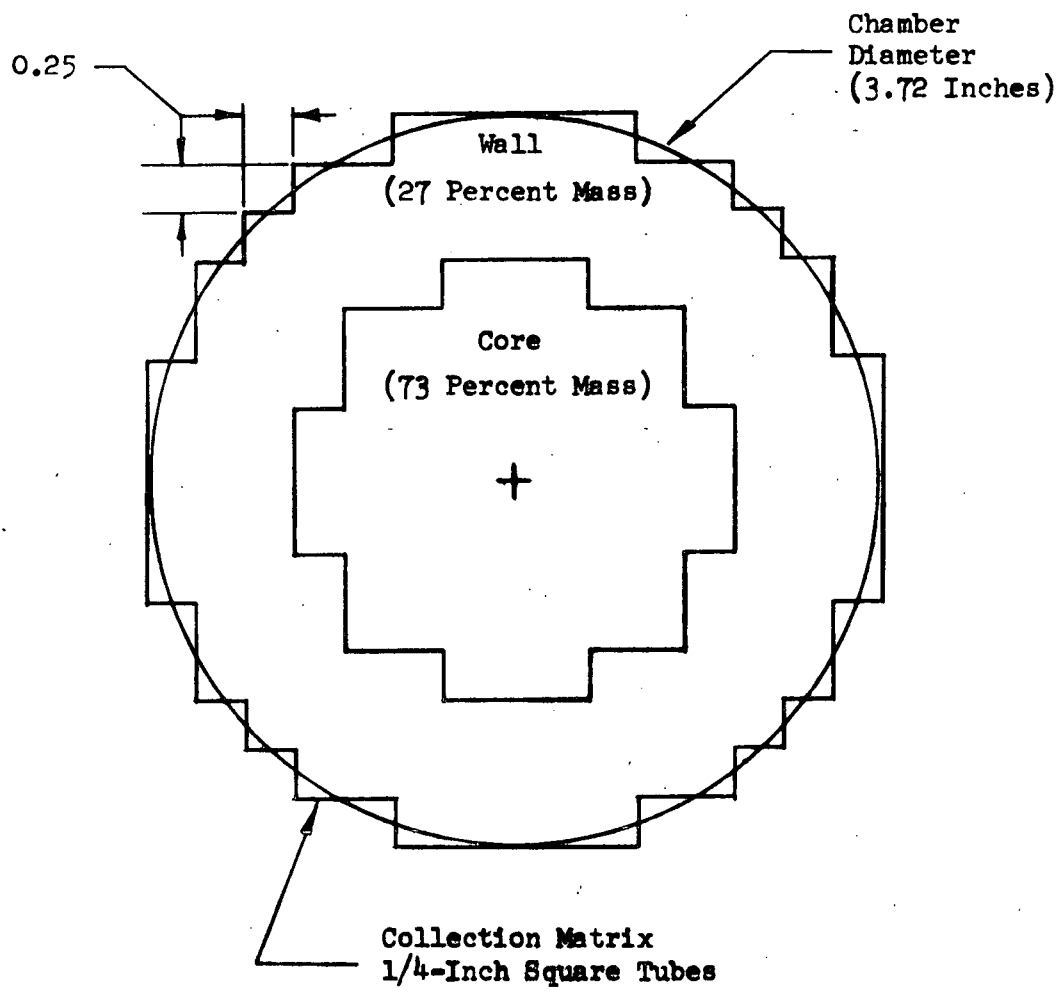


Figure 19. Cold-Flow Collection Matrix

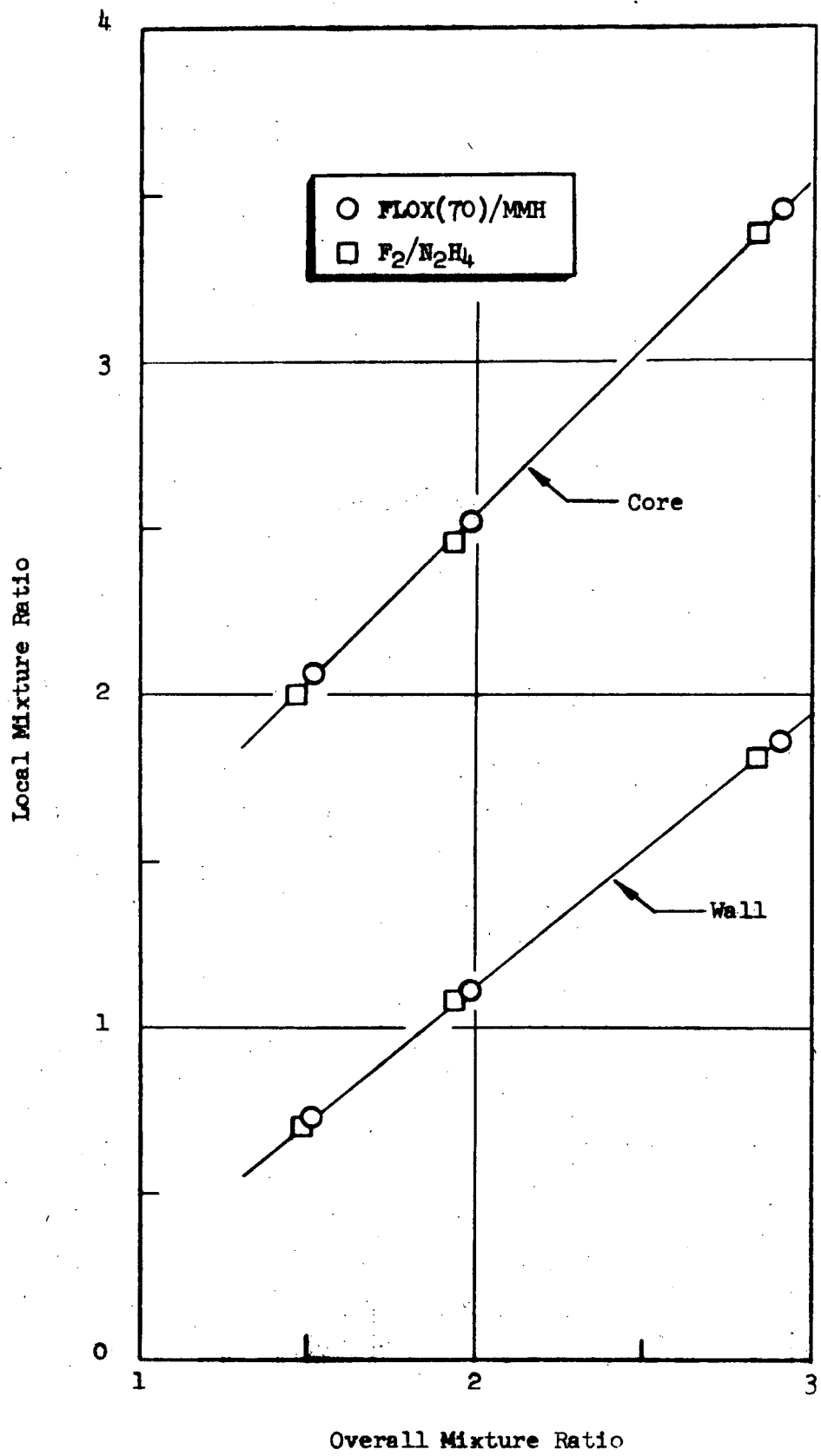


Figure 20. Core and Wall Mixture Ratios vs. Overall Mixture Ratio for Injector No. 1

THERMAL AND EROSION ANALYSES

Throat film coefficients and heat transfer rates were computed using the simplified method of Bartz (Ref. 4). The calculations were made for both FLOX(70)/MMH and F_2/N_2H_4 using combustion gas properties at the wall mixture ratio. The results shown in Fig. 21, however, are plotted versus overall mixture ratio.

The results indicate only a small difference in predicted heat transfer between the propellant systems. The F_2/N_2H_4 film coefficients are slightly lower than those for FLOX(70)/MMH at corresponding mixture ratios, but the heat flux is somewhat higher, reflecting the effect of higher combustion gas temperature.

A one-dimensional thermal ablation program (THAB) was utilized to predict erosion rates of the ATJ graphite throat. Cases were run from 0.5 to 2.5 mixture ratio for FLOX(70)/MMH, F_2/N_2H_4 (anhydrous), and F_2/N_2H_4 (0.5 percent water). The latter case was of interest since the N_2H_4 to be used in the long duration firing contained this amount of water. (Military specifications allow for a maximum of 1.5 percent H_2O .) The theoretical film coefficients were used and the results are shown as the solid curves of Fig. 22. (The dashed curves correspond to the experimental h_g for F_2/N_2H_4 .) The predicted erosion rates were found to differ widely for the FLOX and F_2 systems. For F_2/N_2H_4 (anhydrous) the carbon-hydrogen reaction is the only significant one in the fuel-rich periphery, whereas for FLOX(70)/MMH and F_2/N_2H_4 -water systems the carbon-water reaction will also occur. The rather peculiar shape of the FLOX(70)/MMH curve results from the increasing formation of H_2O at mixture ratios above about 1.1. It is obvious that a relatively low mixture ratio at the injector periphery is an absolute necessity for this propellant combination. The same would not seem to be the case for F_2/N_2H_4 since the predicted erosion rates are roughly the same at mixture ratios of 1.0 and 2.0. The latter value is very close to the optimum kinetic mixture ratio; hence, it would appear that a non-biased injector operating at 2.0 o/f could provide some increase in delivered performance while maintaining a relatively low level of erosion. This, of course, presumes that the graphite would maintain its structural integrity at the higher gas temperatures, which is unlikely.

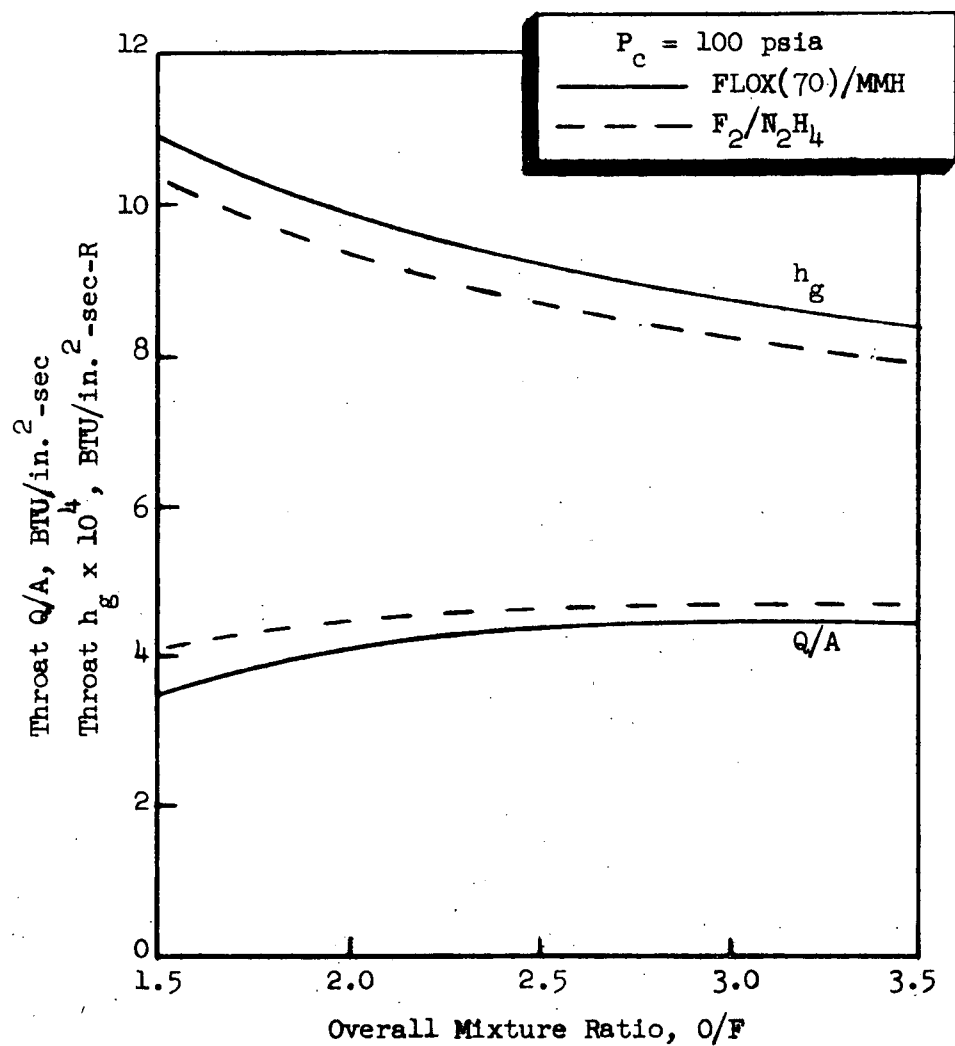


Figure 21. Bartz Theoretical Film Coefficient and Heat Flux at Throat for FLOX(70)/MMH and F_2/N_2H_4

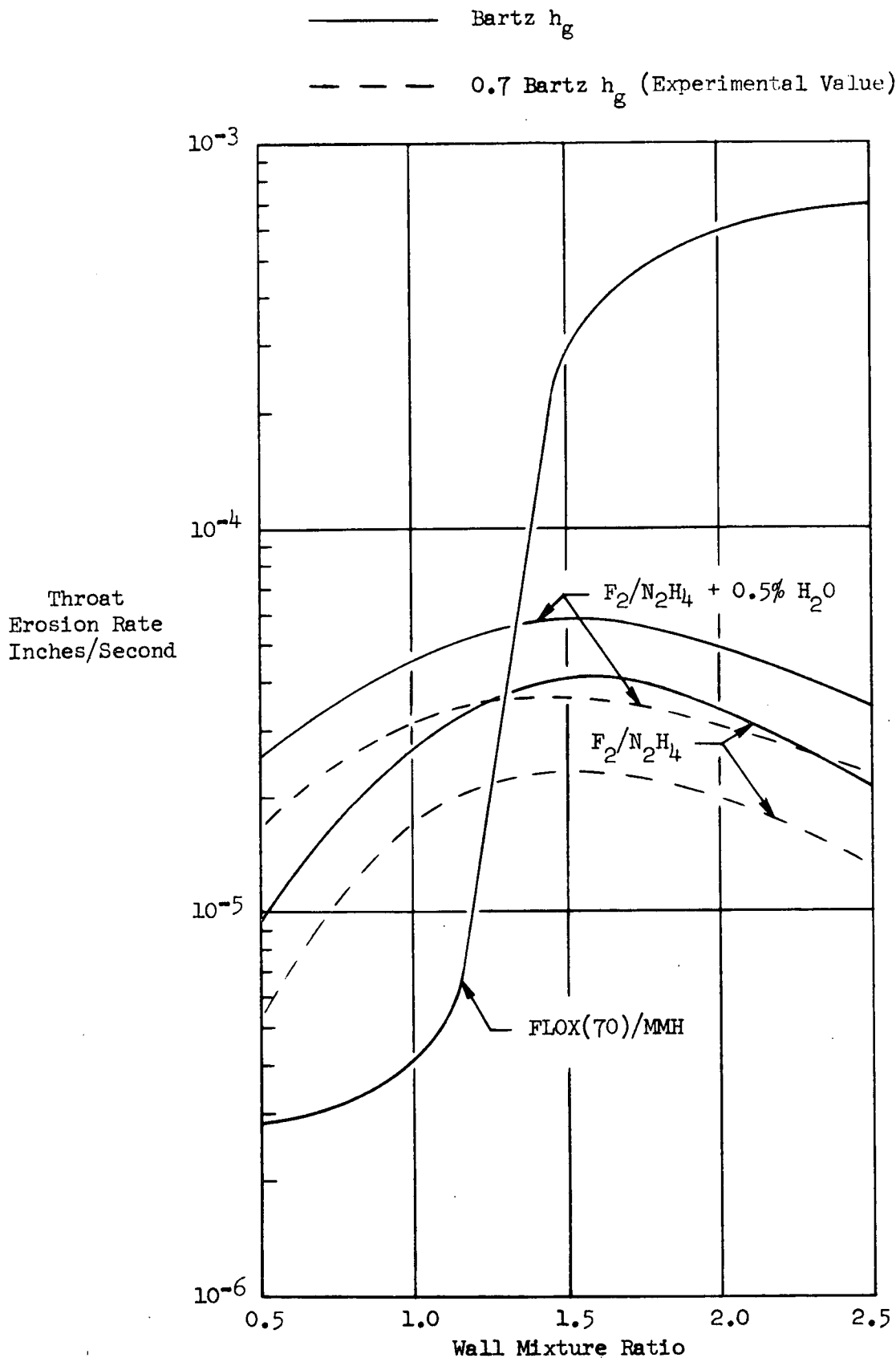


Figure 22. Predicted Throat Erosion Rates

The results of the cold flow experiments and thermal analysis indicated that high performance and minimal erosion rates would be experienced with F_2/N_2H_4 when operating in the range of about 1.5 to 2.0 mixture ratio.

CALORIMETER HOT FIRINGS

A series of short-duration (3 seconds) tests were made with FLOX(70)/MMH and F_2/N_2H_4 to determine comparative performance and heat transfer levels. The number 2 injector and copper chamber were used throughout this test series. The fully instrumented calorimeter assembly is shown in Fig. 23.

The planned test matrix included three firings each for the two propellant combinations at 100 psia chamber pressure and mixture ratios of 1.5, 2.0, and 3.0. Four firings were conducted with FLOX/MMH; only one firing was conducted with F_2/N_2H_4 due to N_2H_4 freezing problems. This one test, conducted at a 2.0 mixture ratio, provided sufficient data for comparison with FLOX(70)/MMH and selection of the operating point for the demonstration test. Test data are presented in Table 2 (Runs 1 through 5).

FLOX(70)/MMH

Four calorimeter firings were conducted with FLOX(70)/MMH (Runs 1 through 4, Table 2). Characteristic velocity (c^*) was calculated using the expression

$$c^* = \frac{P_o A_t g}{\dot{W}_t}$$

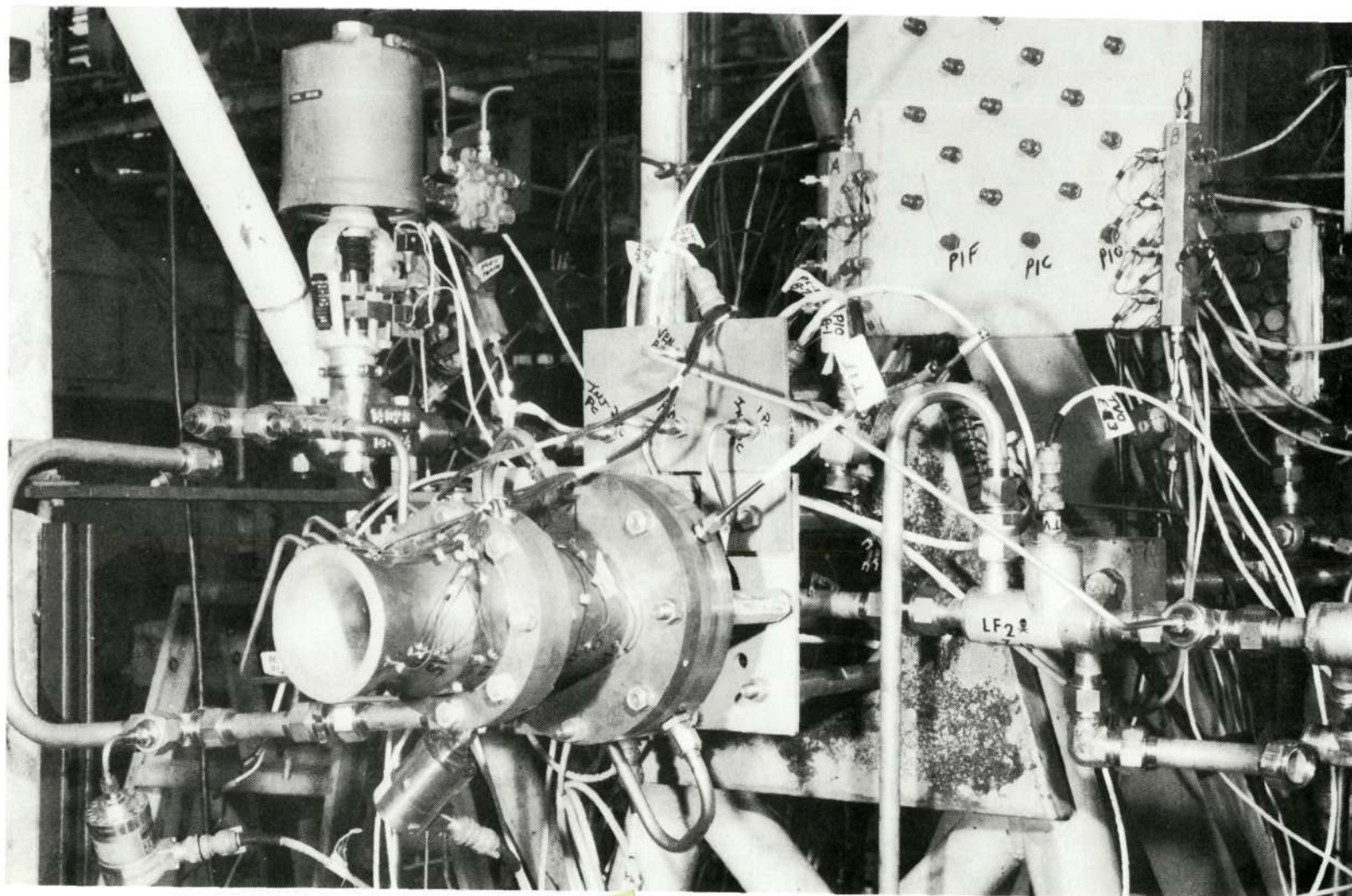
where

P_o = throat stagnation pressure, psia

A_t = throat area, 5.067 in²

g = gravitational constant, 32.174 ft/sec²

\dot{W}_t = total propellant flowrate, lb_m/sec



Reproduced from
best available copy.

5AA24-11/29/71-S1C

Figure 23. Copper Calorimeter Chamber Installation

TABLE 2. HOT-FIRE DATA SUMMARY

Run	1	2	3	4	5	6	7	8
Propellants	FLOX(70)/MMH				F_2/N_2H_4		FLOX(70)/MMH	
Injector	2	2	2	2	2	2	1	2
Chamber	Calorimeter	Calorimeter	Calorimeter	Calorimeter	Calorimeter	Ablative	Ablative #1	Ablative #2
Duration, sec	3	3	3	3	3	500	15	15
P_c , psia	99	96.84	99.88	97.29	101.06	103.89	104.67	106.82
\dot{W}_{ox} , lb/sec	1.625	1.628	1.567	1.969	1.683	1.706	1.816	1.818
\dot{W}_{fu} , lb/sec	0.882	0.857	1.000	0.652	0.832	0.874	0.888	0.883
M.R., o/f	1.84	1.90	1.57	3.02	2.02	1.95	2.04	2.06
ΔP_{ox} , psid	131	130	107	185	122	100	145	131
ΔP_{fu} , psid	122	113	159	63	89	106	127	105
F_{vac} , lb	*	692	704	681	720	759	739	751
c^*_{meas} , ft/sec	*	6333	6323	6032	6530	6696	6311	6449
I_{vac} , sec	*	278.6	274.4	259.9	286.2	294.1	273.4	278.1
η_{c^*} , meas, %	*	94.60	94.58	92.24	92.33	93.78	94.36	96.42
η_{c^*} , cor, %	*	96.37	96.35	94.14	94.57	---	---	---
$\eta_{I_{vac}}$, %	*	91.88	90.73	87.77	89.35	91.79	90.25	91.86

* Steady-state conditions not achieved during Run 1.

Specific impulse efficiency ($I_{s,vac}$) was determined by

$$I_{s,vac} = \frac{F_{vac}}{\dot{W}_t}$$

$$F_{vac} = F_{meas} + P_{amb} A_{exit}$$

where

$$F_{meas} = \text{measured thrust, lb}_f$$

$$P_{amb} = \text{ambient pressure, psia}$$

$$A_{exit} = \text{nozzle exit area, in}^2$$

The stagnation pressure at the throat was calculated using the lowest pressure on the cylindrical chamber pressure profile ($X = 7.5$ inch), and a one-dimensional isentropic expression of the form:

$$\frac{P_o}{P_s} = \left(1 + \frac{\gamma-1}{2} M^2\right)^{\frac{\gamma}{\gamma-1}}$$

where

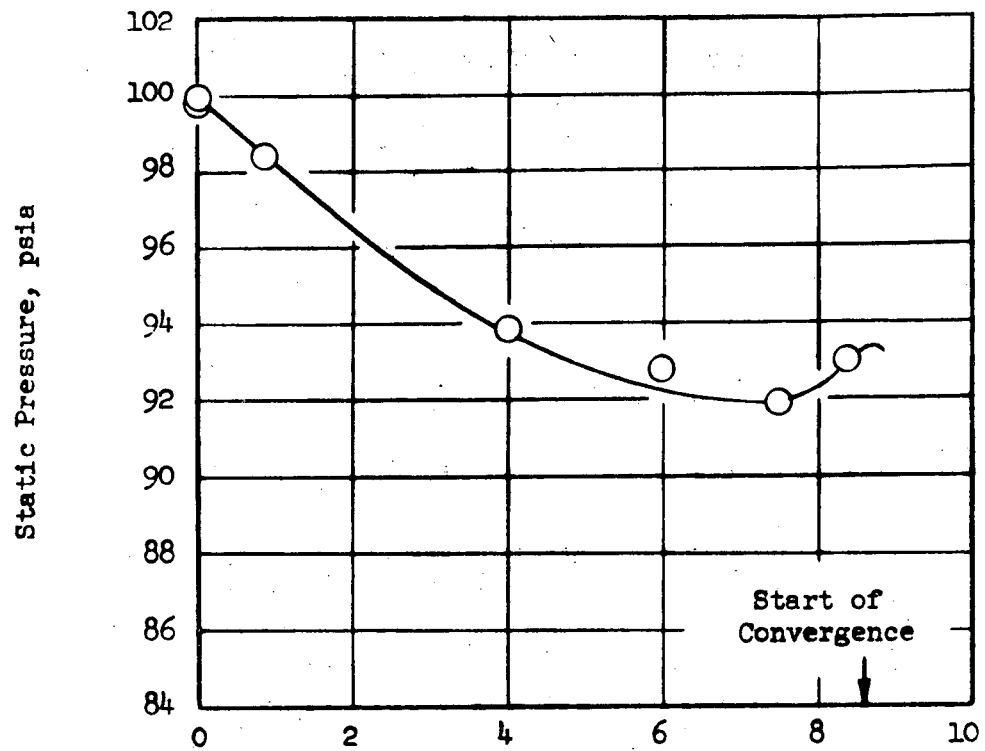
$$P_o = \text{stagnation pressure at throat}$$

$$P_s = \text{static pressure at } X = 7.5 \text{ inch}$$

$$\gamma = \text{ratio of specific heats}$$

$$M = \text{Mach number at point of measurement of } P_s$$

Typical pressure and pressure ratio profiles are shown in Fig. 24. The pressure ratio profile was constant over the 1.57 to 3.02 range of mixture ratio. The primary purpose of measuring the profile was to experimentally determine the ratio of measured injector face pressure (P_f) to the calculated throat stagnation pressure



Run No. 2, $P_c = 96.84$ psia, M.R. = 1.90

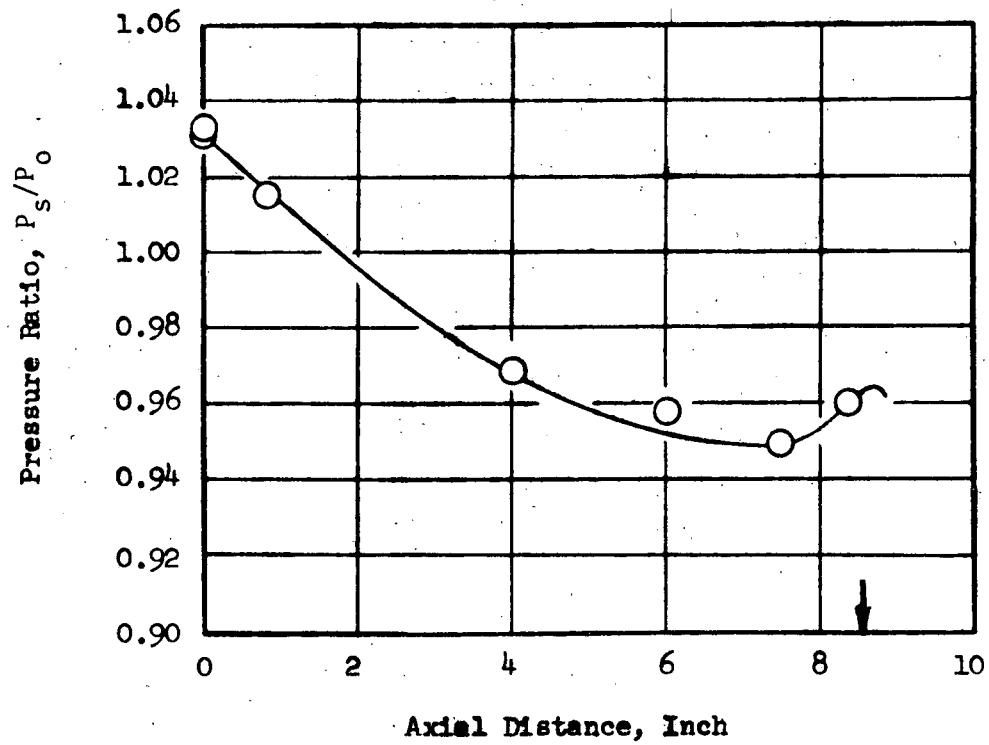


Figure 24. Measured Wall Static Pressure Profile for FLOX(70)/MMH

(P_o) since wall pressures were not measured during the ablative firings. For the FLOX(70)/MMH firings conducted, the ratio P_f/P_o was 1.032.

C* efficiency vs mixture ratio is shown in Fig. 25, with both the measured and corrected values plotted. The corrected values include heat loss influence only, which was the method used in the Ref. 1 program (other correction factors are negligible). A comparison at a 2.0 mixture ratio shows good agreement with the previous results. This plot shows that c* performance was relatively unchanged over the range of 1.5 to 2.0, with lower values at the higher mixture ratios.

The results of the Ref. 1 study (previously shown in Fig. 2) indicate that beyond a chamber length of 10 to 11 inches, performance remains relatively unchanged (for a mixture ratio of 2.0). This implies that propellant vaporization and burning are completed at this point, hence, for the long chamber lengths, performance is "distribution limited." For the like-doublet injector, the performance loss resulting from maldistribution is 3 percent.

The results of the current study, during which mixture ratio was the variable of interest, provide further insight into the combustion process. Over the range of 1.5 to 2.0 mixture ratio, the cold-flow $\eta_{c^*,mix}$ and hot-fire η_{c^*} (corrected) are in agreement. However, at a mixture ratio of 3.0, the hot-fire η_{c^*} is about 3 percent lower than $\eta_{c^*,mix}$, which implies incomplete propellant vaporization. To improve c* efficiency at the higher mixture ratio, it would be necessary to improve propellant atomization and/or increase chamber length.

Specific impulse efficiency is also plotted in Fig. 25. This shows the same basic trend as the c* results; however, the performance decay at both high and low mixture ratios is more pronounced.

Calculated chamber wall heat transfer for the four firings is presented in Fig. 26 and 27. Circumferential heat flux uniformity is evidenced, which coincides with the injector cold-flow data.

Propellants: FLOX(70)/MMH
 Chamber Length: 10.32 in
 Chamber Pressure: 96.84 to 99.88 psia
 Injector No. 2

X Corrected c^* Efficiency Obtained
 in NAS7-304 Program Using
 Similar Hardware

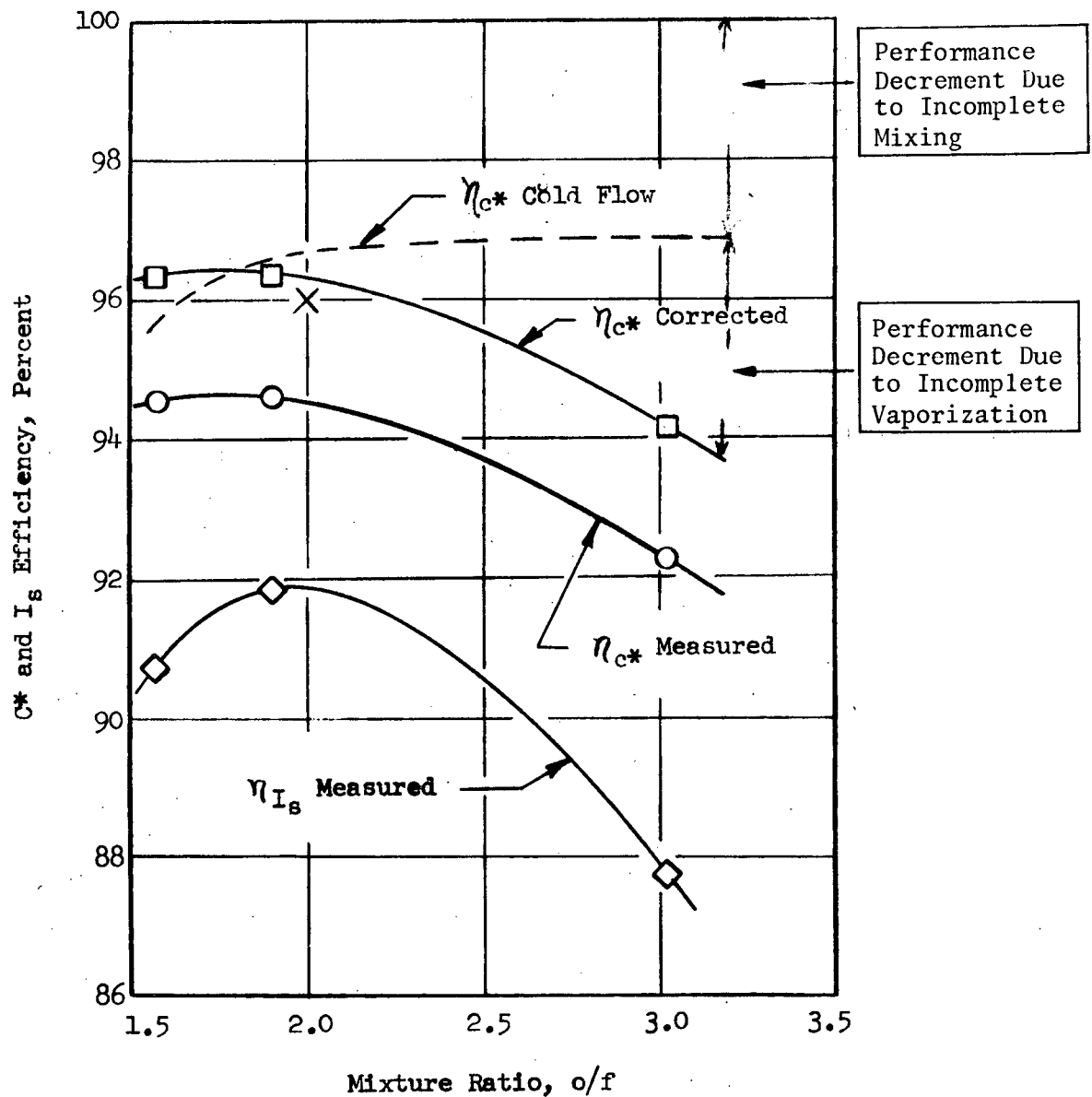


Figure 25. C^* and $I_{s_{vac}}$ Efficiency for FLOX(70)/MMH

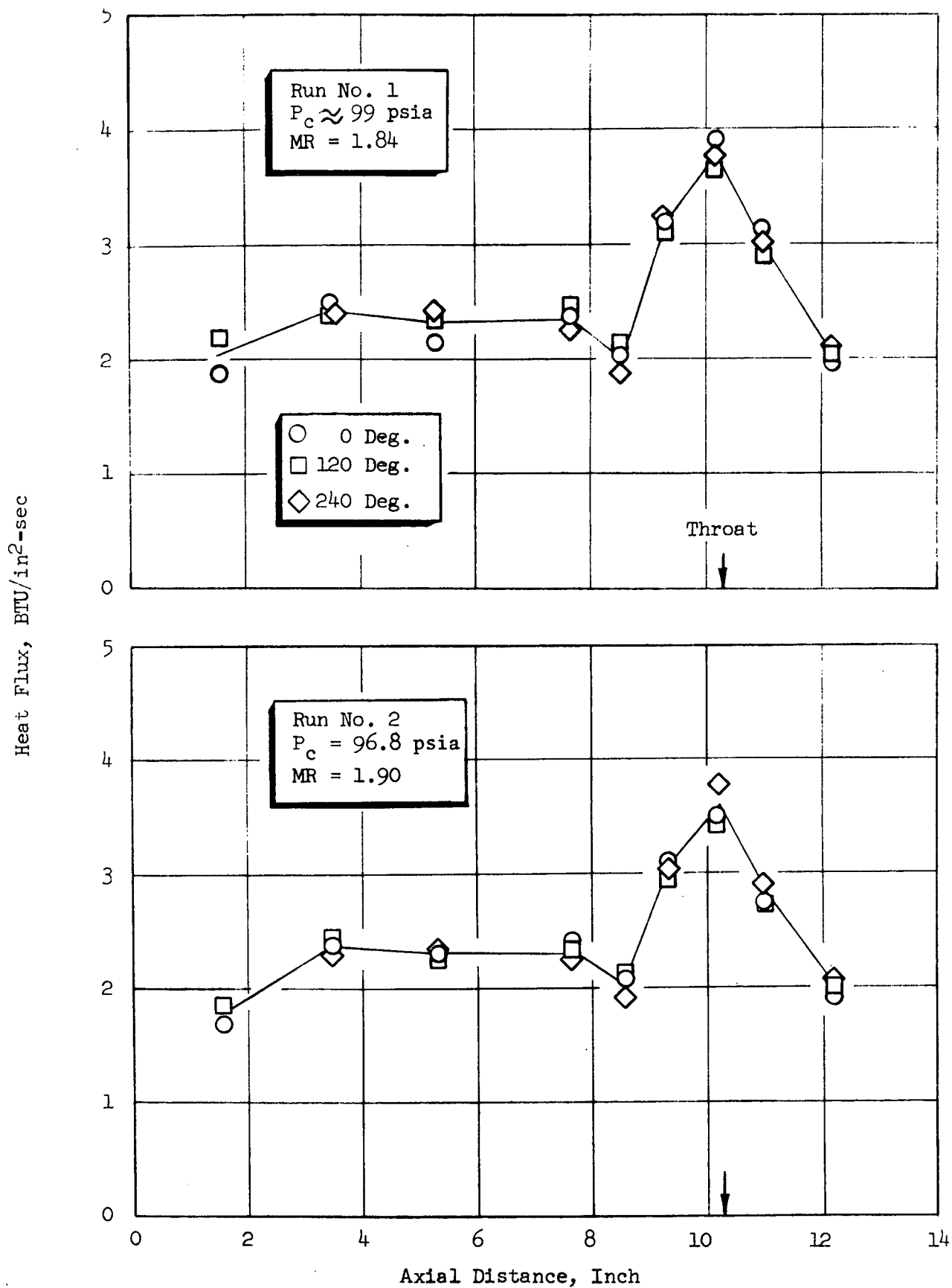


Figure 26. FLOX(70)/MMH Chamber Wall Heat Flux for Run Nos. 1 and 2

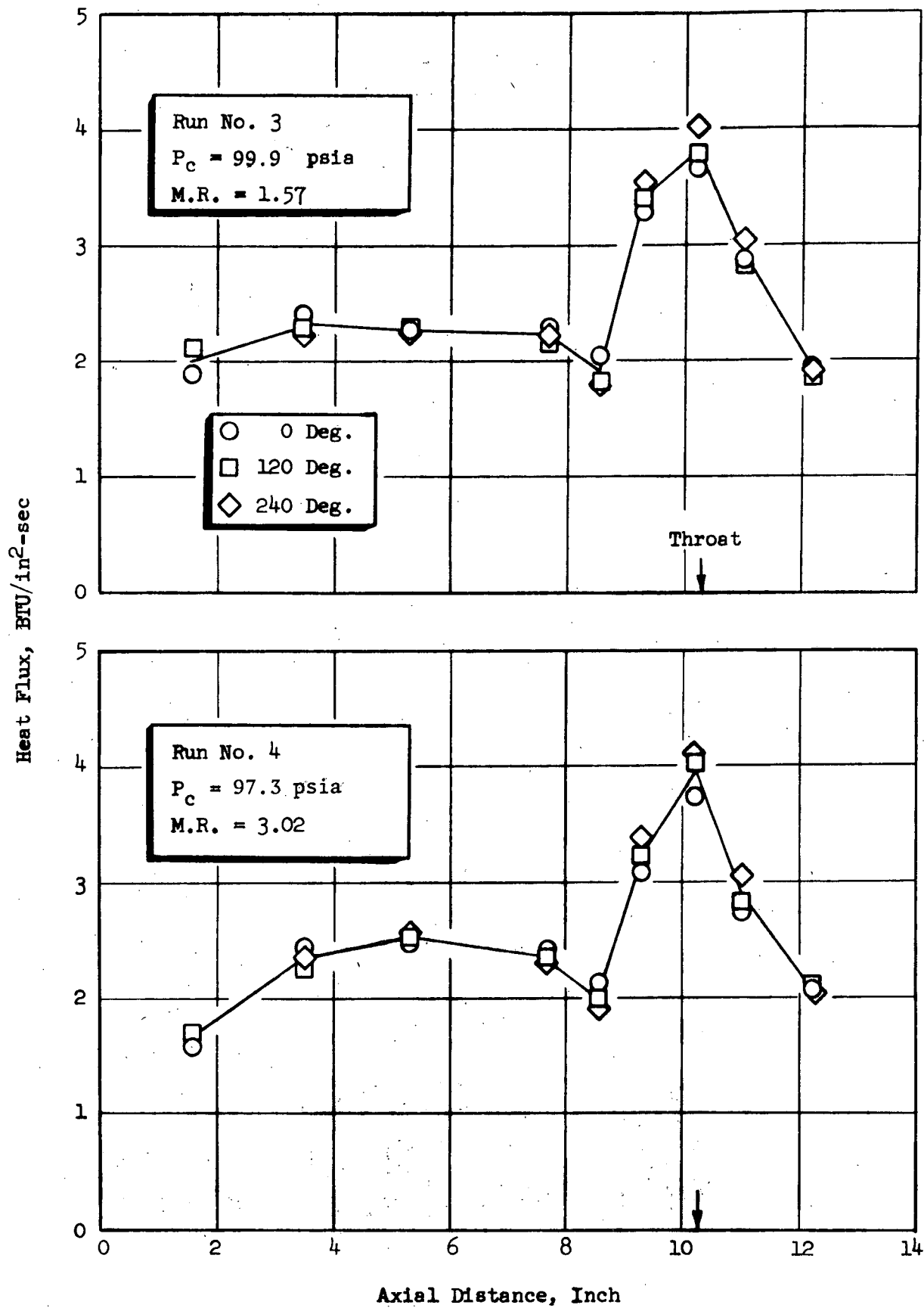


Figure 27. FLOX(70)/MMH Chamber Wall Heat Flux for Run Nos. 3 and 4

Calculated throat heat flux and film coefficients are plotted vs mixture ratio in Fig. 28. Experimental heat flux (Q/A) was computed by

$$\frac{Q}{A} = \frac{w C_p}{A} \frac{dT_H}{d\theta}$$

where w = weight of thermal isolation segment, lb_m
 C_p = specific heat of segment, Btu/lb_m-F
 A = area of segment, $in.^2$
 $\frac{dT_H}{d\theta}$ = rate of change of hot-side temperature with time, F/sec

For a low Biot modulus ($Bi \leq 0.1$), it can be shown that

$$\frac{dT_c}{d\theta} \approx \frac{dT_H}{d\theta}$$

hence, the heat flux can be calculated directly from the measured cold-side temperature data. Film coefficients (h_g) were computed by

$$h_g = (Q/A)/(T_{aw} - T_w)$$

$$T_{aw} = \eta_{c*}^2 T_g$$

where T_g = theoretical gas temperature at the wall mixture ratio, R
 T_w = calculated hot-side wall temperature, R
 T_{aw} = adiabatic wall temperature, R
 η_{c*} = measured c^* efficiency

The data have been normalized to 100-psia chamber pressure by the expression

$$Q/A, h_g \propto P_c^{0.8}$$

Also shown are the predicted values of h_g and Q/A as computed by the simplified method of Bartz (Ref. 4). The coefficients were calculated using combustion gas

properties at the wall mixture ratio, but the data are plotted versus overall mixture ratio. The experimental results were within 10 percent of the values predicted by the Bartz equation.

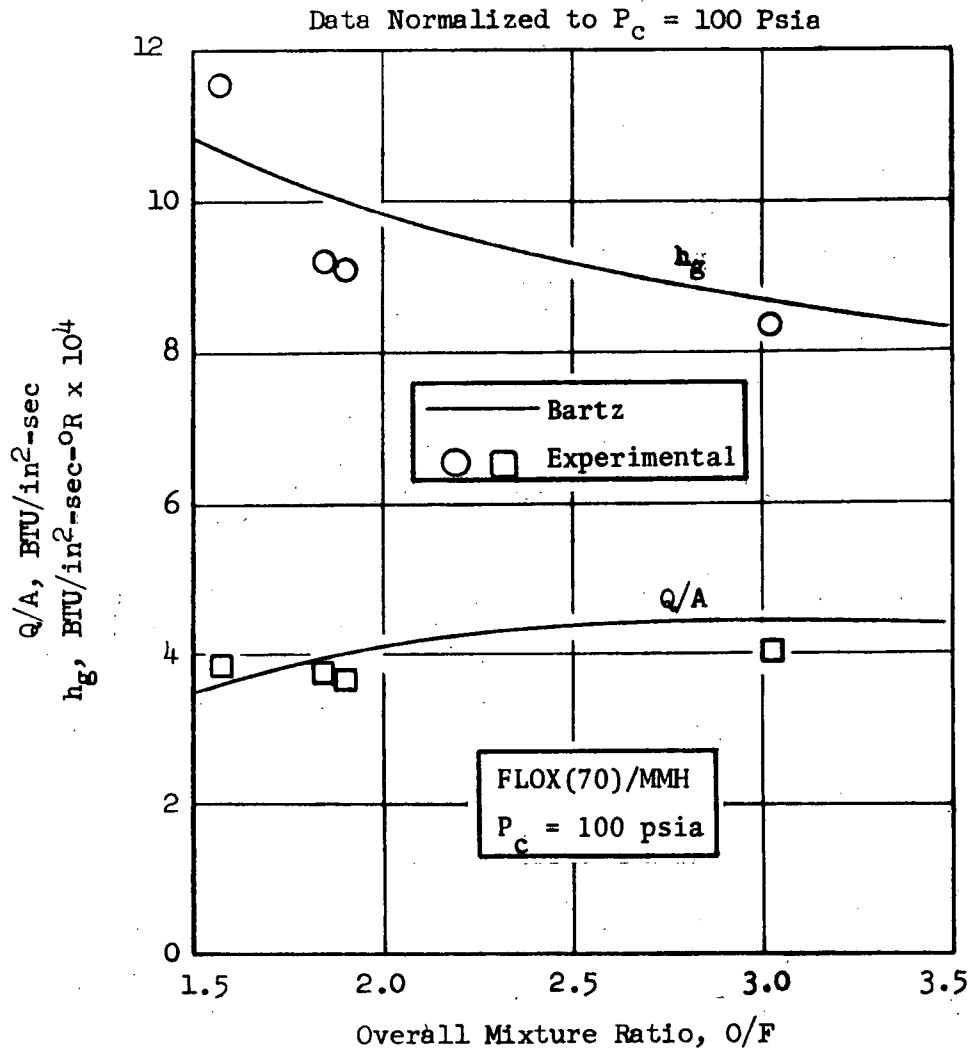
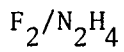


Figure 28. Throat Heat Flux and Film Coefficient for FLOX(70)/MMH



The original plan was to hot-fire F_2/N_2H_4 over a mixture ratio range of 1.5 to 3.0 to provide a basis of comparison with FLOX(70)/MMH. The initial attempt at firing with a liquid nitrogen prechilled injector resulted in freezing the N_2H_4 in the fuel manifold. In fact, the N_2H_4 froze so rapidly that there was no evidence of ignition, even though there was full F_2 flow through the injector.

The liquid nitrogen pre-chill procedure was therefore eliminated during future tests. Also, gaseous nitrogen purges through the injector manifolds were not initiated until immediately prior to propellant valve opening to achieve near-ambient temperature in the fuel manifold. This latter procedure was considered necessary since ambient (and fuel) temperature was 47 F which is only 13 F above freezing for N_2H_4 .

The ambient temperature start resulted in a successful test of 3 seconds duration (Run 5, Table 2). This time, however, the N_2H_4 froze after the run was completed. This situation was caused by the relatively cold nitrogen post-test gas purge which reached a low temperature of 0 F.

The performance results from this test are summarized in Table 2. The c^* and I_s values were approximately 3 percent higher than those for FLOX(70)/MMH, although the efficiencies were about 2 percent lower. The pressure and pressure ratio profile (Fig. 29) were almost identical to those for FLOX(70)/MMH.

Heat flux data for this test are presented in Fig. 30. As predicted, the F_2/N_2H_4 and FLOX(70)/MMH results were similar, although F_2/N_2H_4 was predicted to result in a somewhat higher heat flux than the FLOX(70)/MMH.

The overall experimental results were encouraging, since performance was high and heat flux low. This, along with the throat erosion predictions, indicated that F_2/N_2H_4 could be expected to yield satisfactory results when using chamber components designed specifically for FLOX(70)/MMH. The F_2/N_2H_4 mixture ratio selected for the long-duration demonstration was 1.90. This corresponds to a wall mixture ratio of about 1.0, with a predicted throat erosion rate of 3.1×10^{-5} inch/second. For a 500-second firing, this would result in an increase in throat area of 2.4 percent.

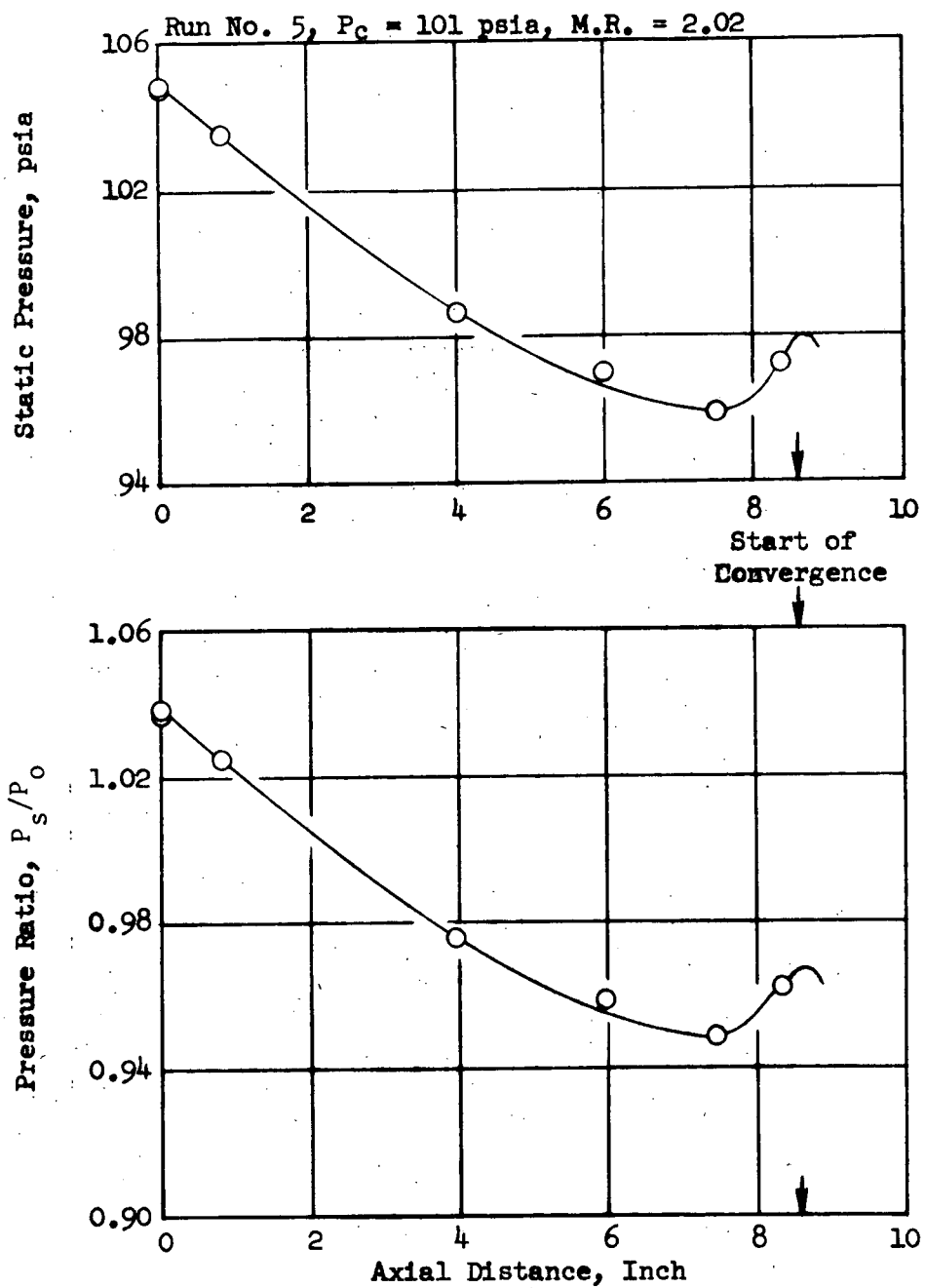
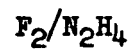


Figure 29. Chamber Wall Pressure Profile for F_2/N_2H_4

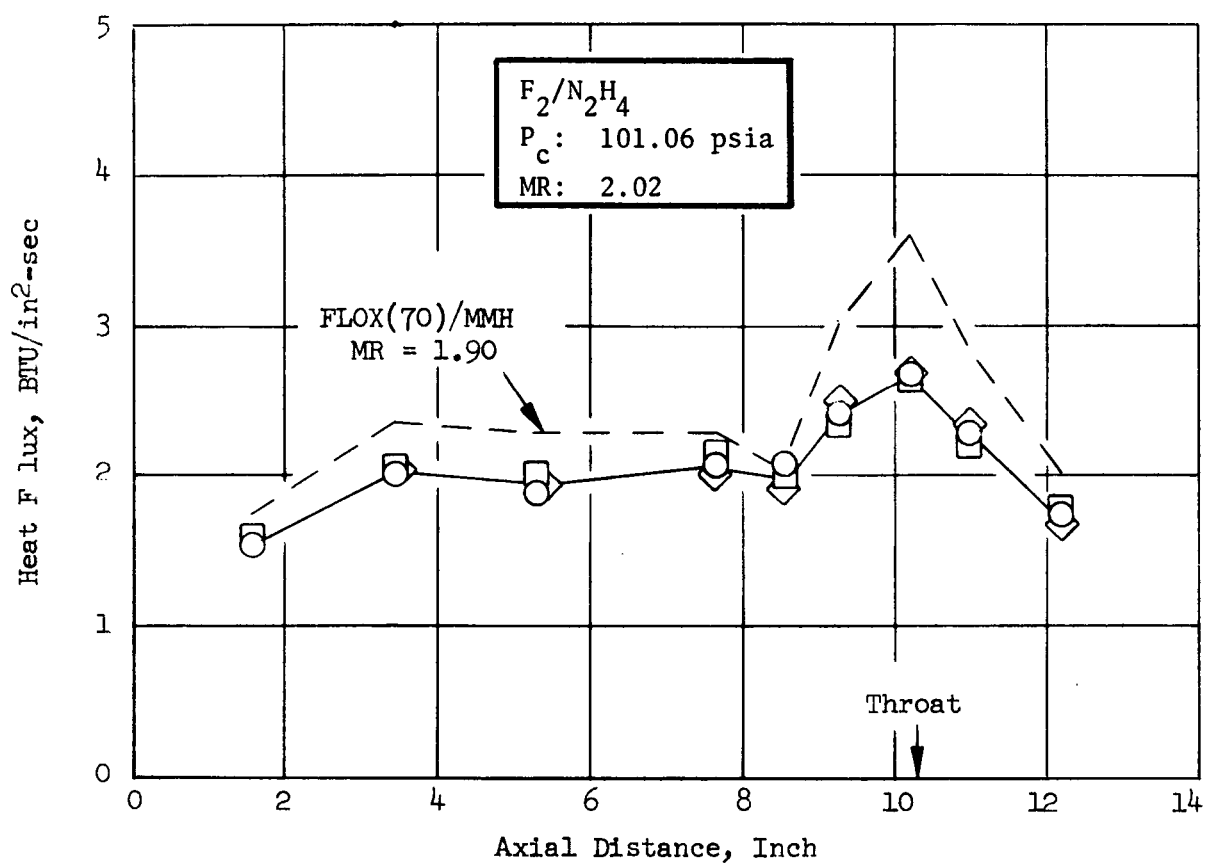


Figure 30. F_2/N_2H_4 Chamber Wall Heat Transfer

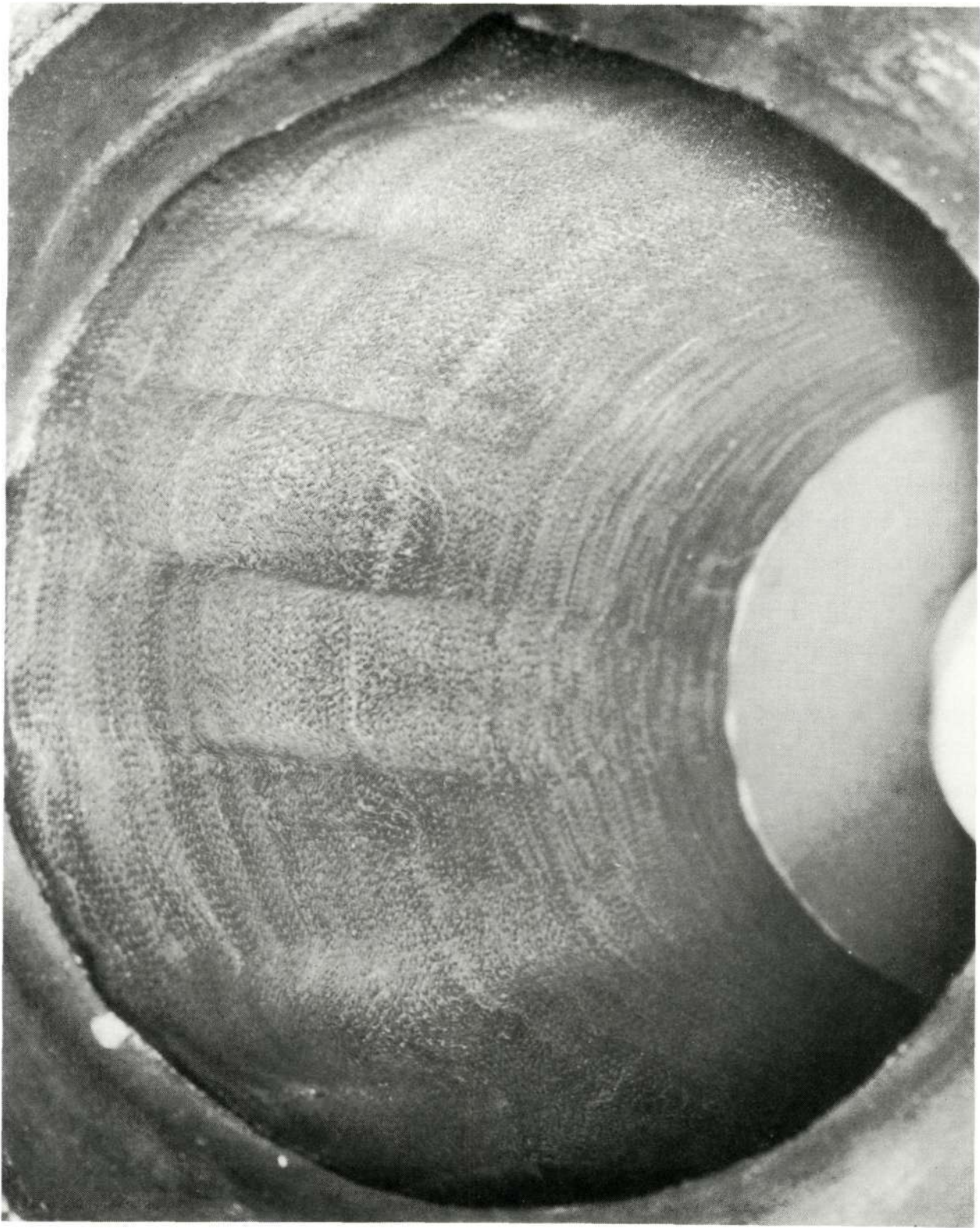
F_2/N_2H_4 DEMONSTRATION FIRING

A 500-second-duration firing was conducted utilizing the same injector used in the calorimeter tests (No. 2) and with the ablative chamber. The performance, summarized in Table 2 (Run 6) showed, as expected, slightly higher (~ 2 percent) uncorrected c^* and I_s than the calorimeter results, which is consistent with the lower heat loss expected with the ablative chamber. Performance was calculated near the end of the test, using the pressure profile shown in Fig. 29 from the calorimeter firing ($P_f/P_o = 1.0376$) and the measured post-test throat area.

The overall durability of the injector and thrust chamber were excellent, as can be seen from the post-test photographs of Fig. 31 through 33. There was a thin brownish colored deposit on the injector face (the injector photograph was taken prior to cleaning) which was suspected to be resin from the ablative material. There was no indication of overheating at any location on the injector face.

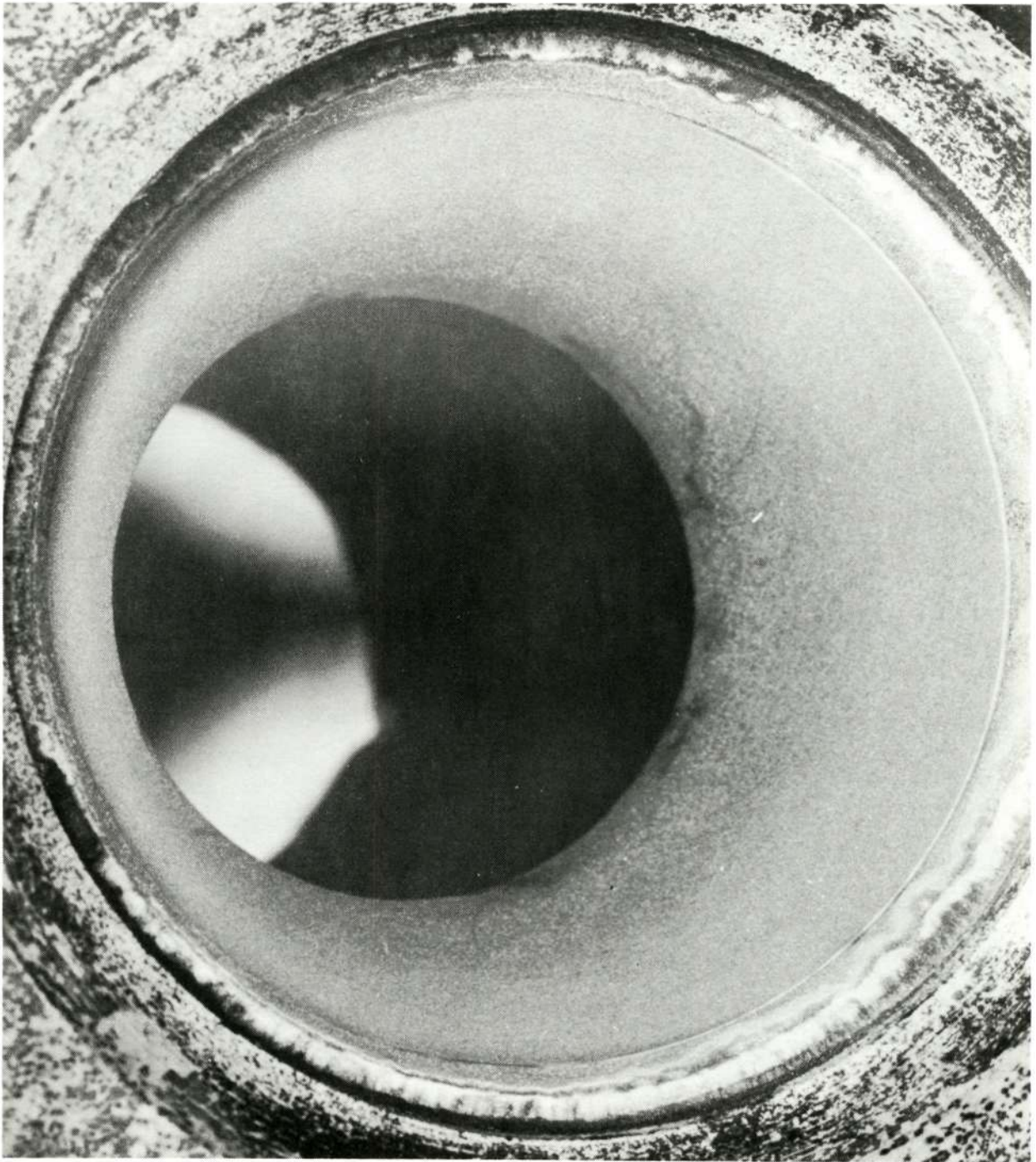
The post-test condition of the ablative is best described by the photograph of Fig. 34. Erosion of the ATJ graphite throat was minimal and very uniform. The throat area increase was 1.75 percent as measured with a micrometer at six circumferential locations. Actual pre-test and post-test measurements are given in Table 3. This corresponds to an erosion rate of 2.5×10^{-5} inch/second which compares well with the predicted value of 3.1×10^{-5} (dashed curve of Fig. 22 for $F_2/N_2H_4 + 0.5\% H_2O$ at wall mixture ratio = 1.0). In addition, there was no sign of cracks or fractures in the throat insert.

Figure 35 shows a similar ablative chamber after a 1000-second firing with FLOX(70)/MMH on Program NAS7-304 (Ref. 2). The carbon/phenolic chamber liner was tape wrapped at a 6-degree angle and resulted in excessive wrinkling. The erosion of the two pressure ports is also evident from this photograph. The erosion pattern produced by these two propellant systems is noticeably different in the chamber liner. From the injector face to a point about 3 inches downstream, there was practically no erosion with FLOX(70)/MMH, whereas F_2/N_2H_4 produced significant erosion in this area. The F_2/N_2H_4 chamber exhibited 16 "scallop" which were in direct radial alignment with the outer ring of oxidizer doublets.



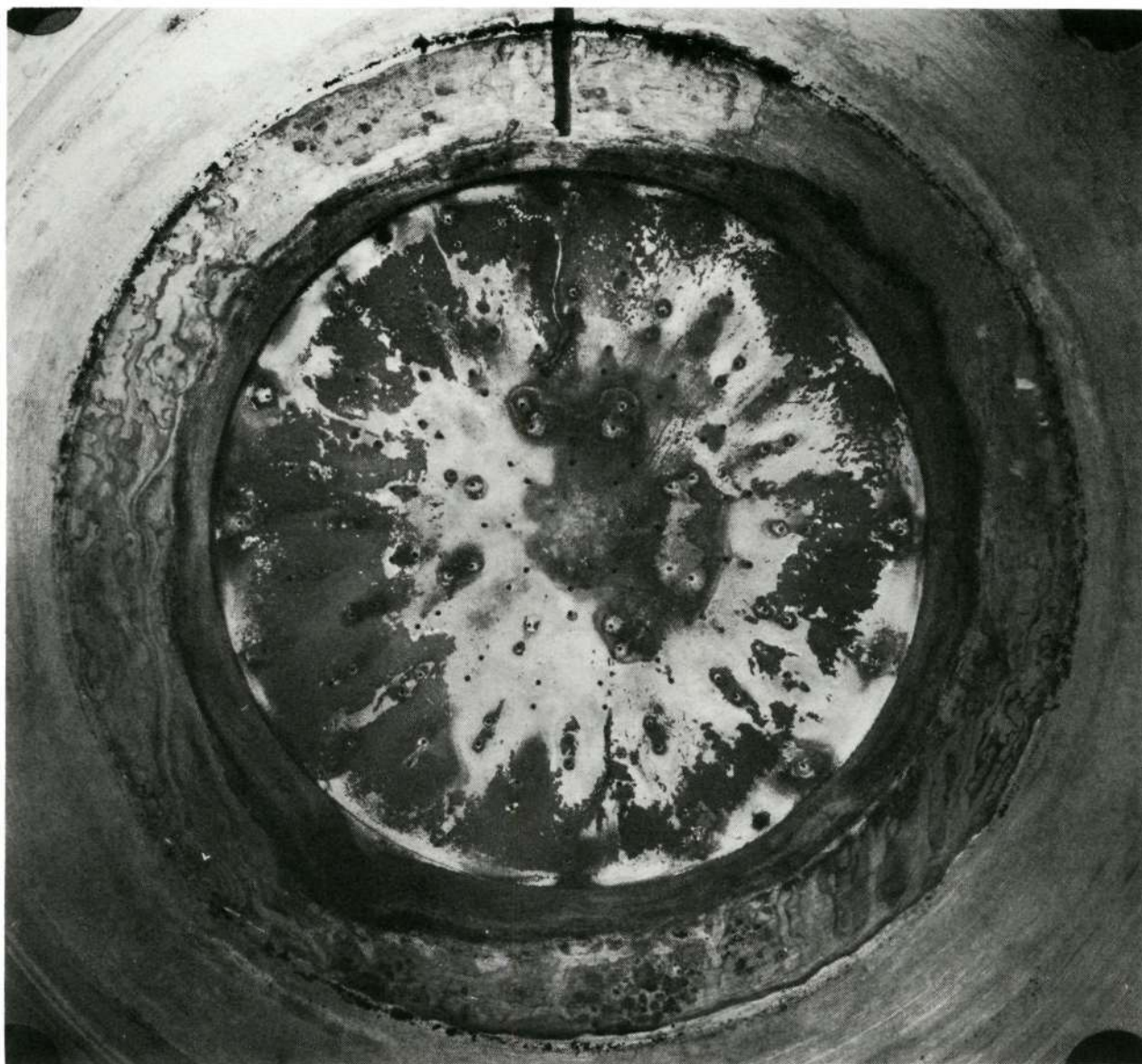
5AA36-12/14/71-S2A

Figure 31. Injector End View of Ablative Chamber After
500-Second Firing with F_2/N_2H_4



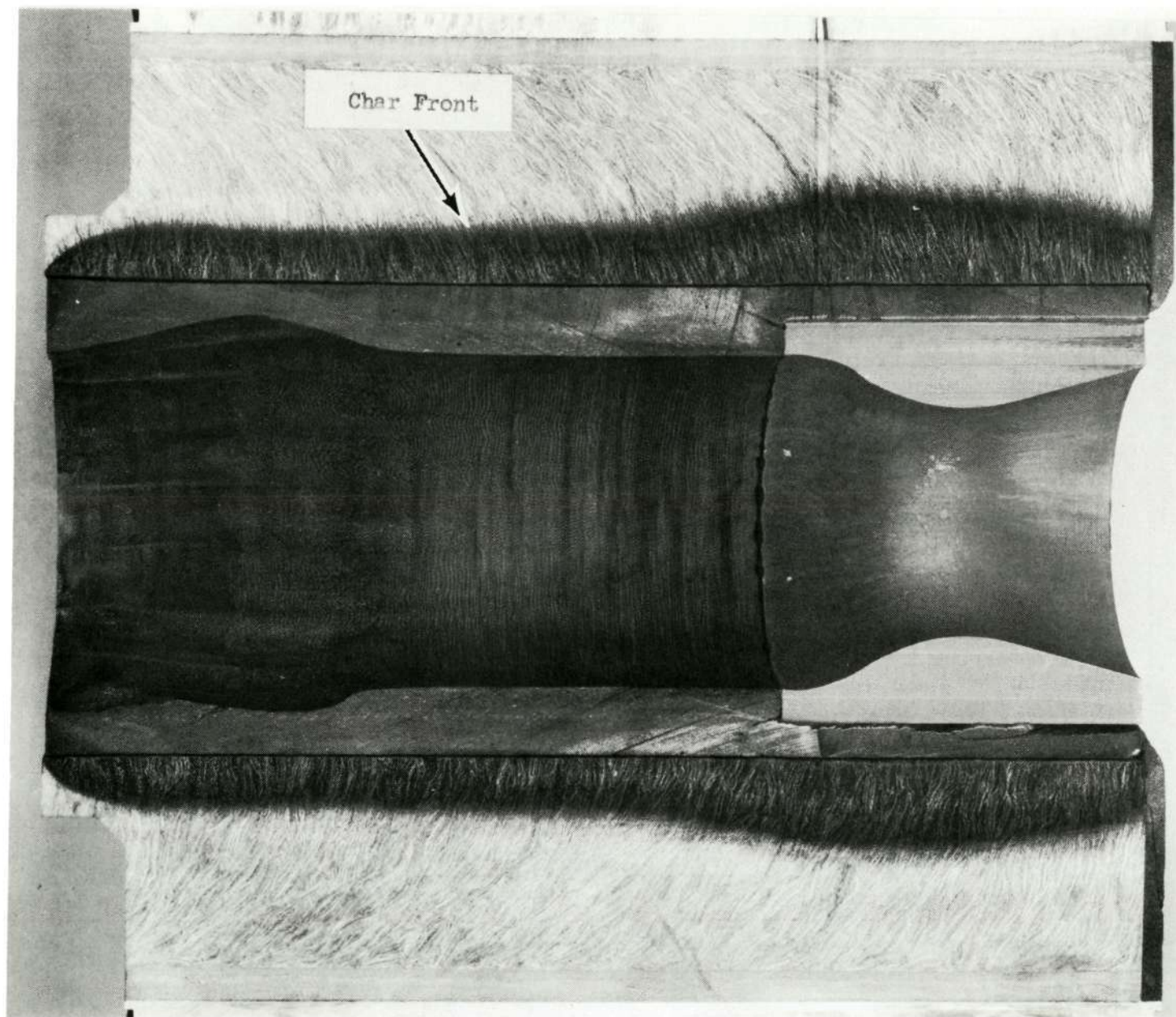
5AA36-12/14/71-S2C

Figure 32. Nozzle End View of Ablative Chamber After
500-Second Firing with F_2/N_2H_4



5AA36-12/14/71-S2B

Figure 33. Self-Impinging Doublet Injector After 500-Second Firing with F_2/N_2H_4 (Prior to Cleaning)



5AA34-12/15/71-C1

Figure 34. Section View of Ablative Thrust Chamber
After 500-Second F_2/N_2H_4 Firing

TABLE 3. ABLATIVE CHAMBER MEASUREMENTS

Position	Chamber Diameter*		Throat Diameter	
	Pre-Test	Post-Test	Pre-Test	Post-Test
12:00	3.717 in.	3.712 in.	2.544 in.	2.566 in.
1:00	3.716	3.715	2.543	2.568
2:00	3.716	3.695	2.541	2.566
3:00	3.716	3.717	2.542	2.563
4:00	-----	-----	2.544	2.564
5:00	-----	-----	2.544	2.564

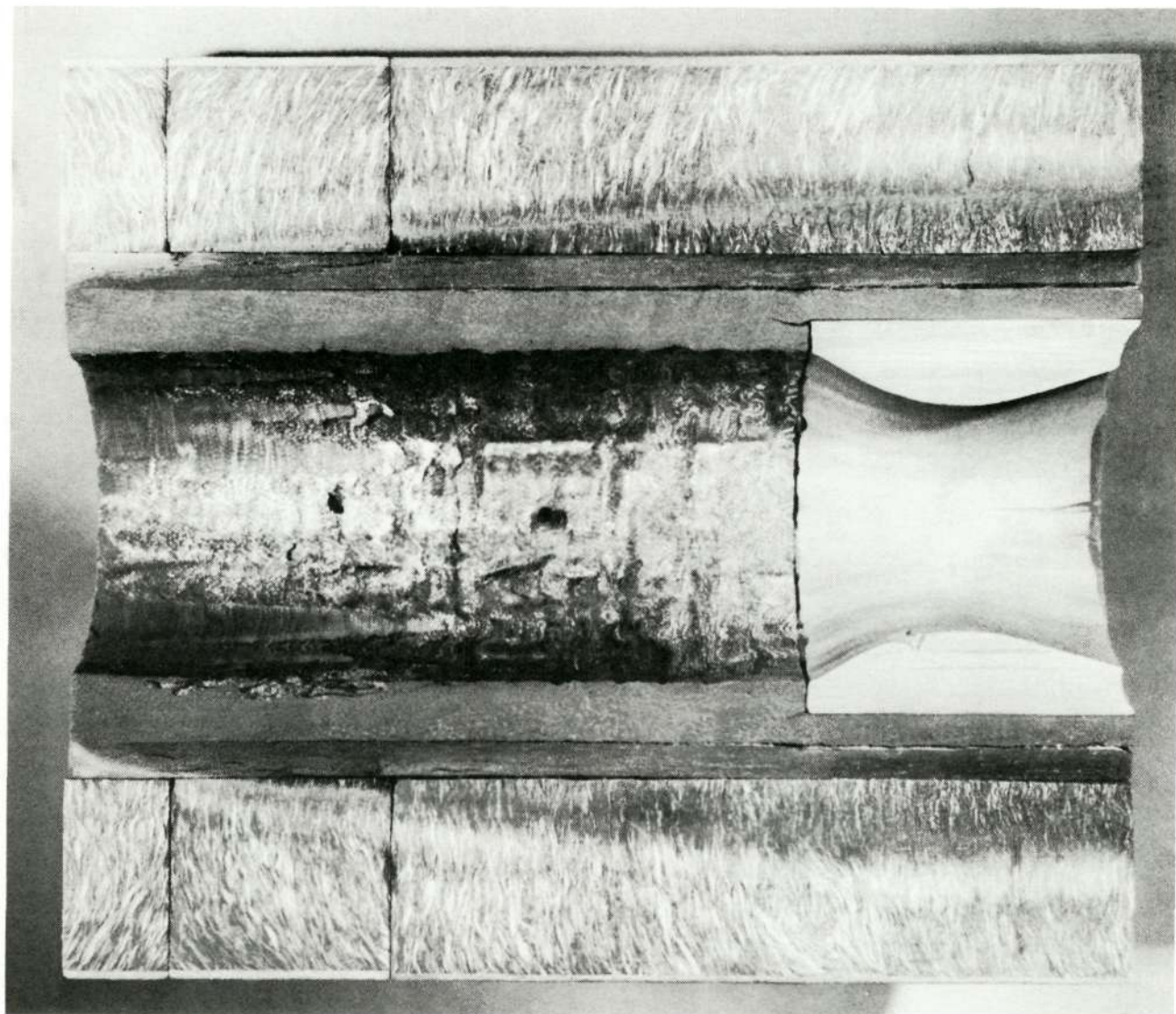
* Measured at 6 in. from injector end.

Pre-Test Area = 5.079 in²

Post-Test Area = 5.168 in²

Percent Increase = 1.75

Reproduced from
best available copy.



5AA36-12/7/67-S1F

Figure 35. Composite Ablative Thrust Chamber After a 1000-Second-Duration Firing with FLOX(70)/MMH (Program NAS7-304)

This would suggest that the locally heavy erosion was caused by a fluorine-carbon reaction. There are two possible explanations: first, the lower temperature associated with FLOX(70)/MMH may limit the wall temperature to a level where the carbon-oxygen reaction is greatly reduced; secondly, if the MMH vaporizes more rapidly than N_2H_4 (consistent with the performance results), this would tend to inhibit the radial outflow of the more rapidly vaporizing oxidizer. The latter would result in a lower mixture ratio near the wall for FLOX(70)/MMH, and correspondingly lower erosion.

The downstream section of the carbon/phenolic liner was virtually erosion free as indicated by the measurements of Table 3.

The modification of the throat insert did not appear to reduce the erosion at the upstream end of the throat. It appears that this is caused by combustion gas leakage, either around the throat insert or through the graphite itself (ATJ graphite is rather porous). The erosion doesn't seem to be large enough to warrant further investigation, but it probably could be reduced by the use of a higher density graphite.

Ablative wall temperature histories at 12 locations (Fig. 9) are presented in Fig. 36 through 39. A maximum temperature of 3800 F was observed at the throat, which is about 600 F higher than previous 1000-second FLOX(70)/MMH firing results. Extrapolation of the F_2/N_2H_4 data to 1000 seconds results in a maximum throat temperature of approximately 4000 F.

HOT-FIRE ACCEPTANCE TESTS

FLOX(70)/MMH acceptance tests were conducted to determine the delivered c^* and I_s performance levels and to demonstrate the structural integrity of the two engine assemblies. Installation of a fully instrumented chamber assembly is shown in Fig. 40. Target operating conditions for these tests were as follows:

Chamber Pressure:	100 psia
Mixture Ratio:	2.0 o/f
Duration:	15 seconds

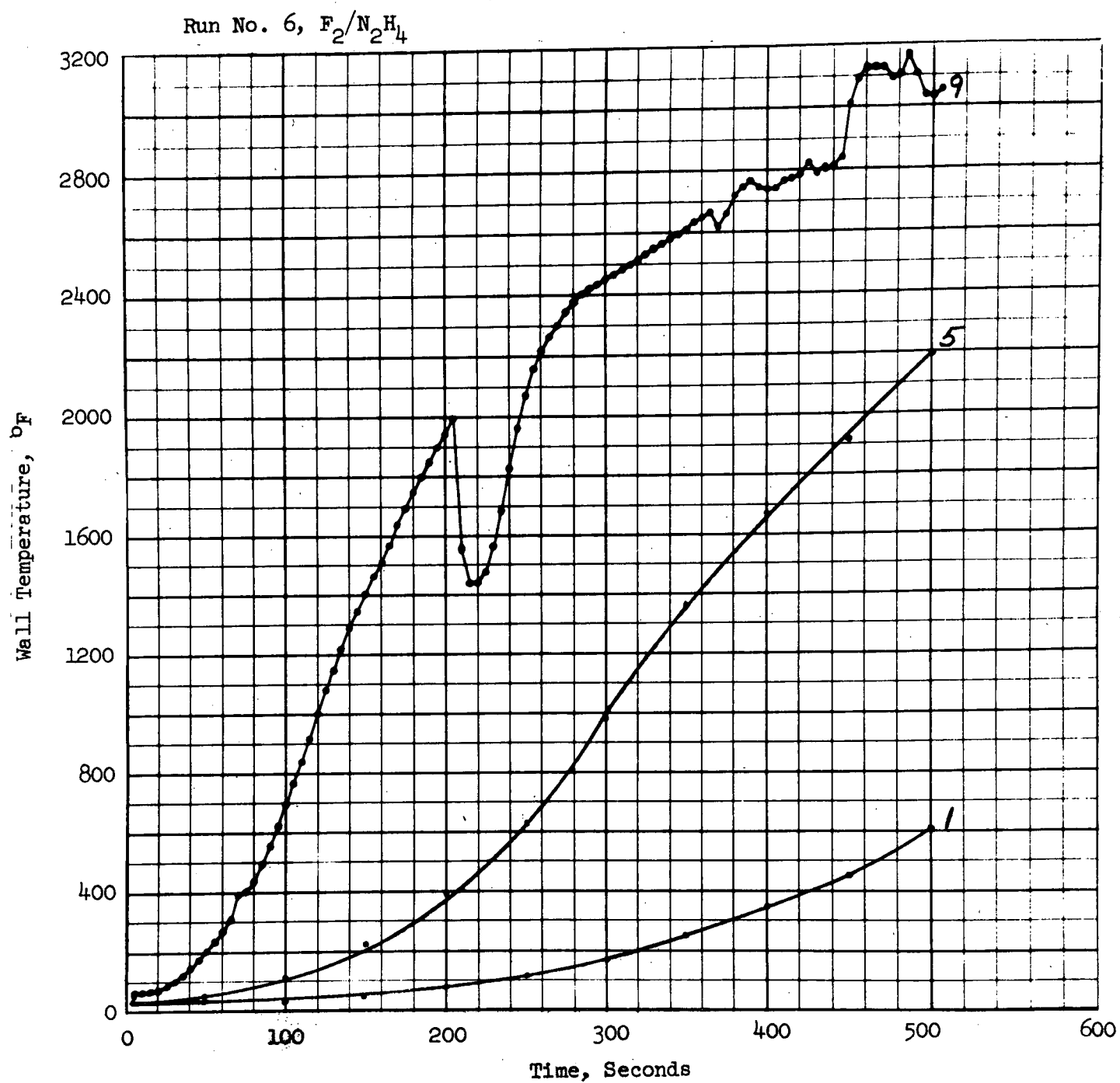


Figure 36. Ablative Chamber Wall Temperature at Positions 1, 5, and 9

Run No. 6, F_2/N_2H_4

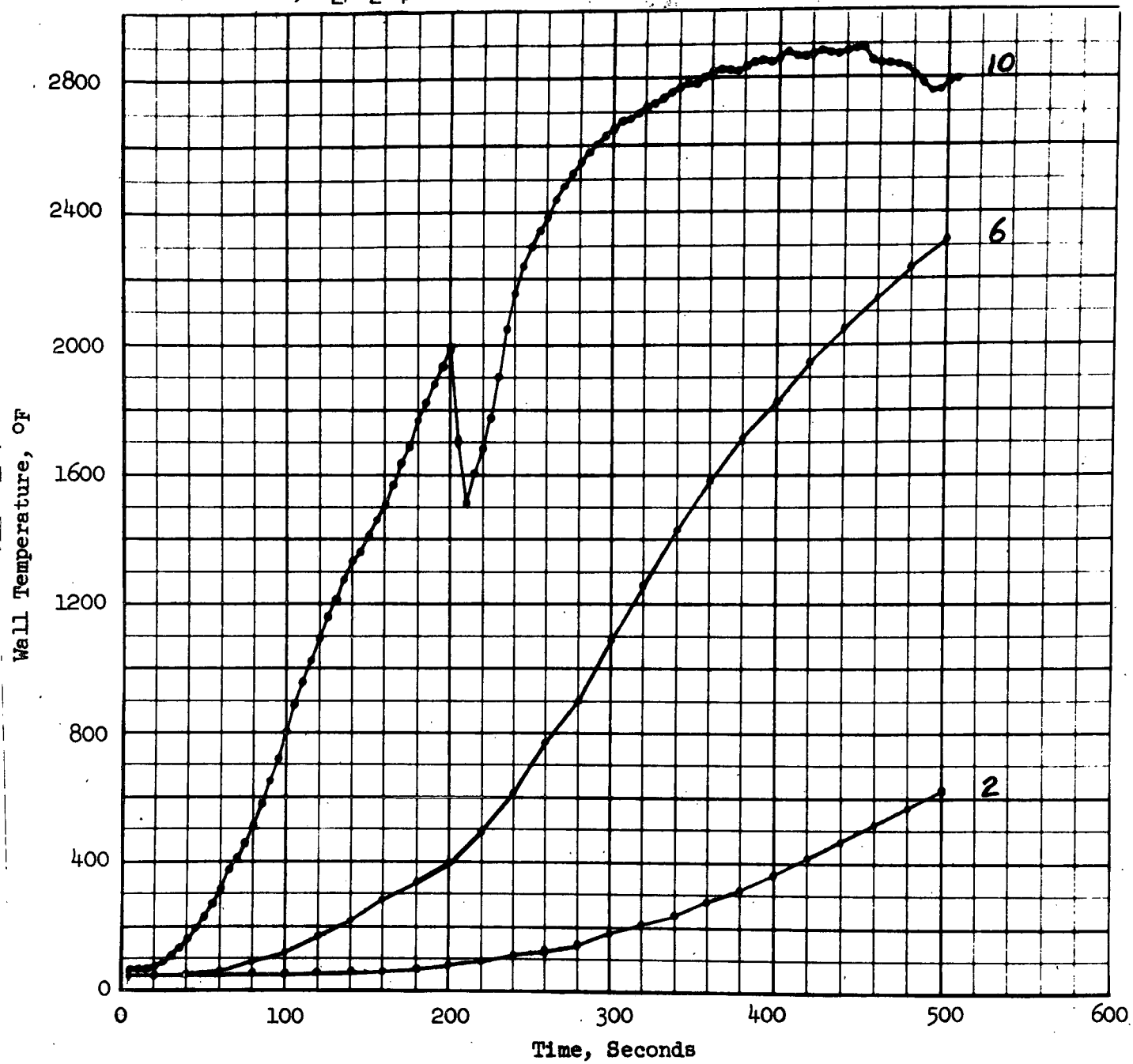


Figure 37. Ablative Chamber Wall Temperature at Positions 2, 6, and 10

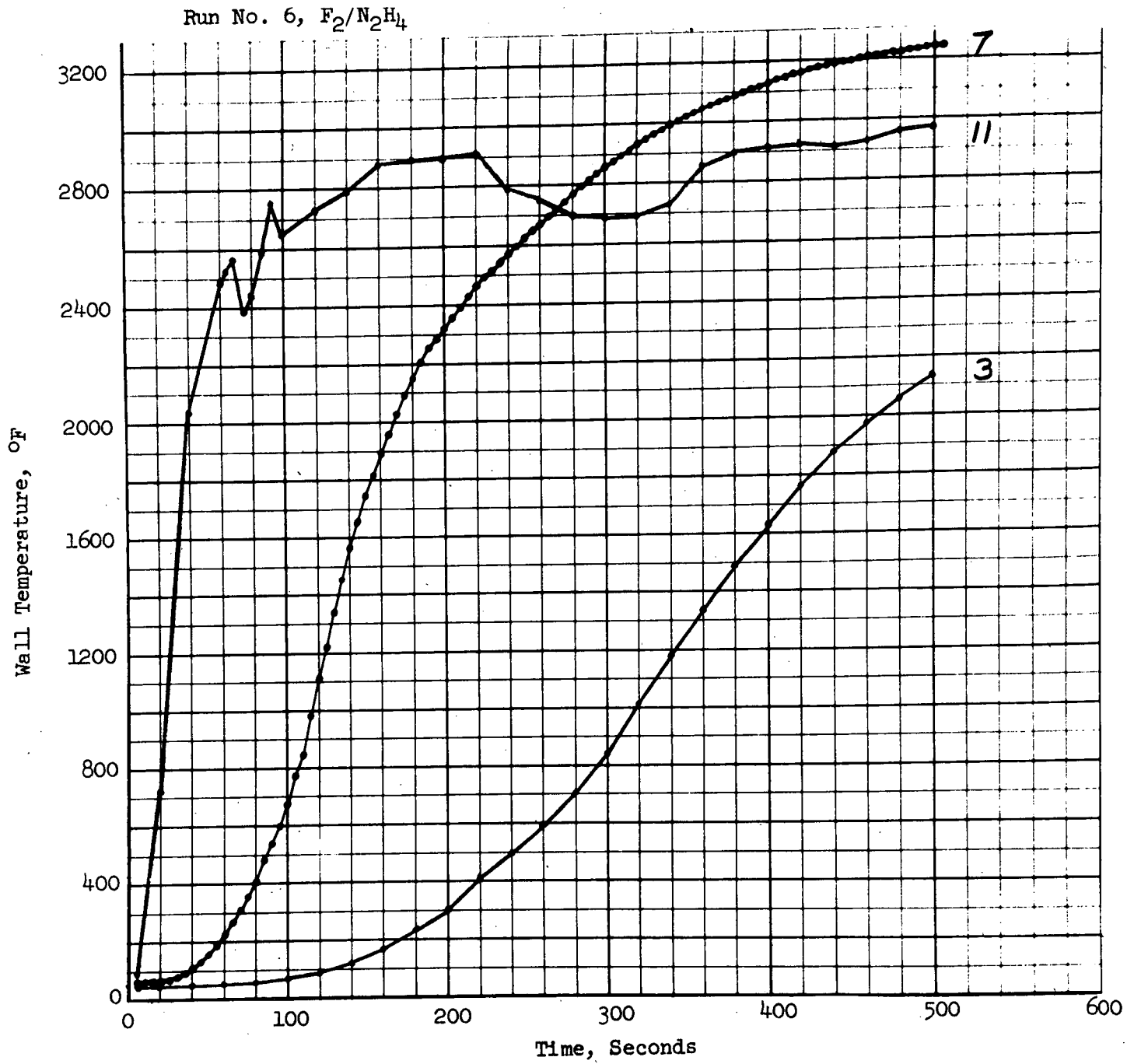


Figure 38. Ablative Chamber Wall Temperature at Positions 3, 7, and 11

Run No. 6, F_2/N_2H_4

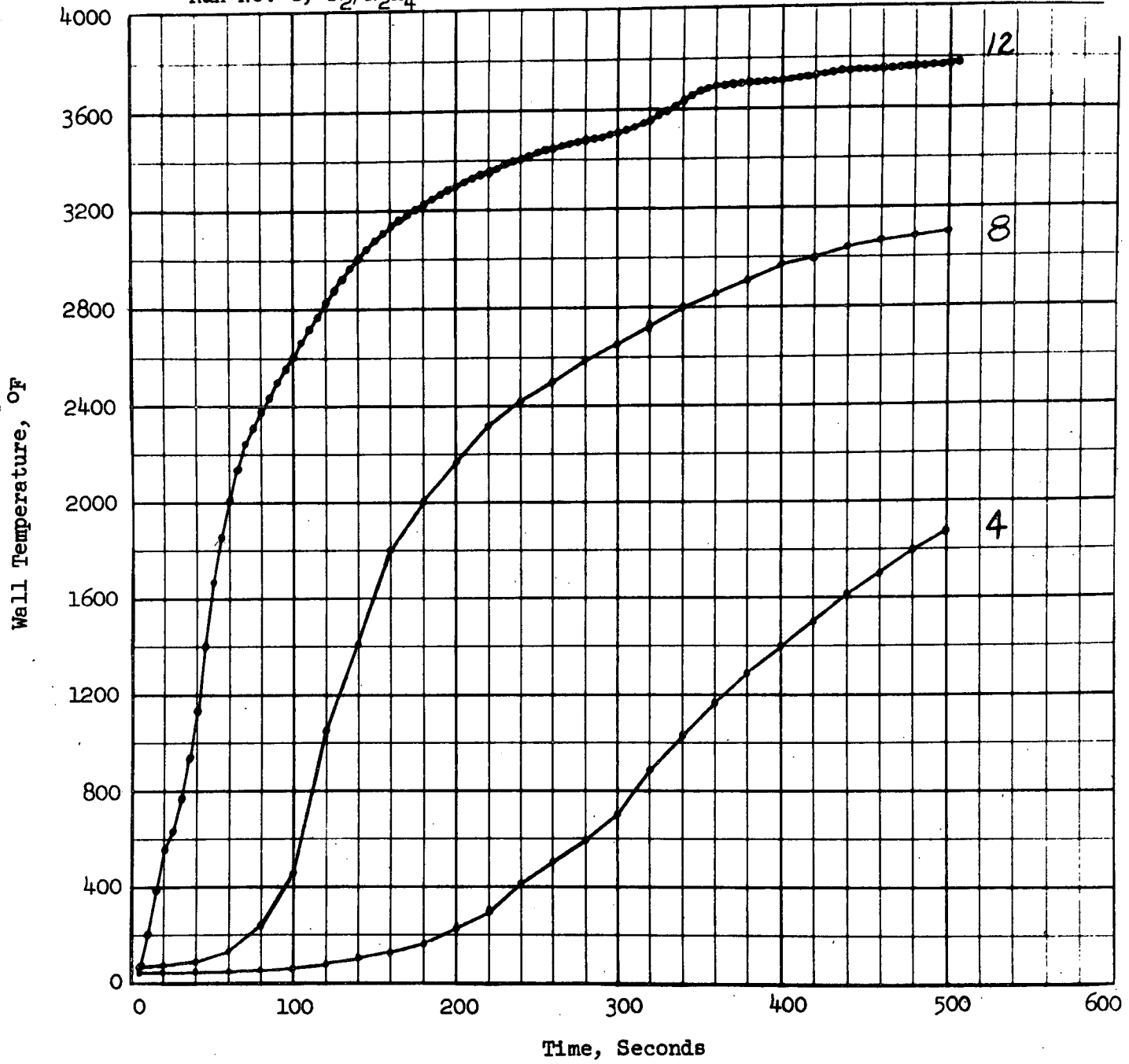
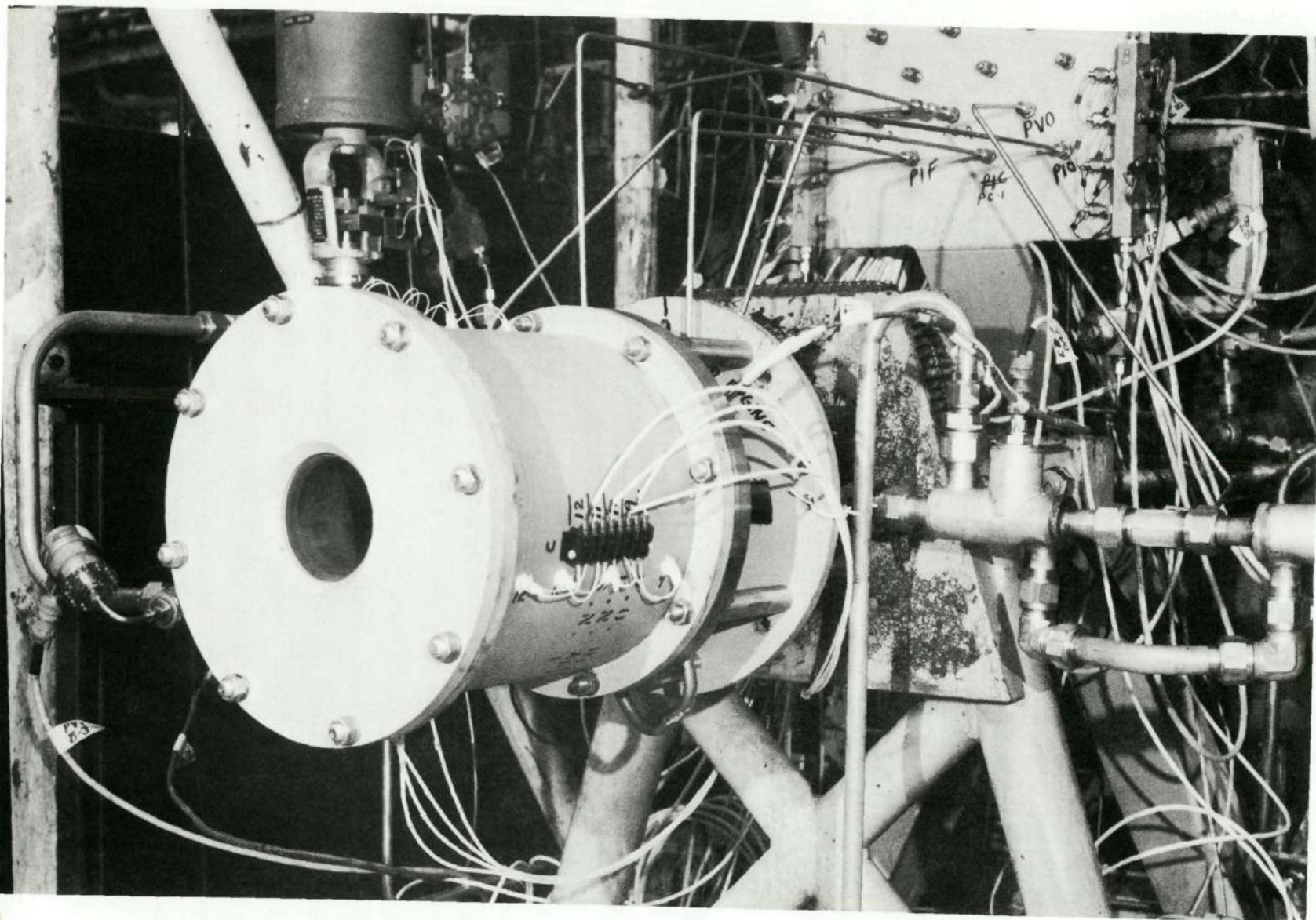


Figure 39. Ablative Chamber Wall Temperature at Positions 4, 8, and 12

Reproduced from
best available copy.



5AA34-12/11/71-S1B

Figure 40. FLOX/MMH R.E.A. Installation

Both tests were initiated with the chamber components at near-ambient temperature. This resulted in a start transient of about 5 seconds before steady-state chamber pressure and thrust were achieved as shown in Fig. 41.

A summary of the test data is given in Table 2 (Runs 7 and 8). Both injectors exceeded the minimum c^* requirement of 6000 ft/sec.

It was expected that the combustion efficiencies for these two heatsink type chamber tests would be similar to the uncorrected c^* levels (~94.5 percent) obtained in the short duration calorimeter firings at mixture ratios in the vicinity of 2.0. This uncorrected performance level was achieved with injector number 1 (94.4 percent). However, the number 2 injector produced an approximately 2 percent higher efficiency (96.4 percent).

A detailed review of the data from the acceptance tests revealed that the fuel side hydraulic characteristics of the number 2 injector were different in that test than in previous tests (Runs 1 - 6). During Run 8 the discharge coefficient for the fuel side was 0.69. In previous tests it had been 0.64 ± 0.01 . The discharge coefficient was constant during the 500-second test (Run 6). Since nickel and the hydrazine family of fuels are not totally compatible, it is possible that some degree of chemical attack occurred after completion of the 500-second firing. This attack at either the fuel orifice entrances or in the orifices themselves may well have caused the observed increase in discharge coefficient. Conditions after the 500-second test were conducive to hydrazine attack because of (1) the heat soakback from the hot ablative chamber to the injector after test completion, and (2) the injector was exposed to hydrazine for an extended period of time (~44 hours) prior to cleaning. This exact procedure had been used many times with FLOX(70)/MMH with no noticeable changes in fuel orifice hydraulics. The relationship between the change in fuel orifice hydraulics and the ~2 percent increase in performance is still, however, unclear.

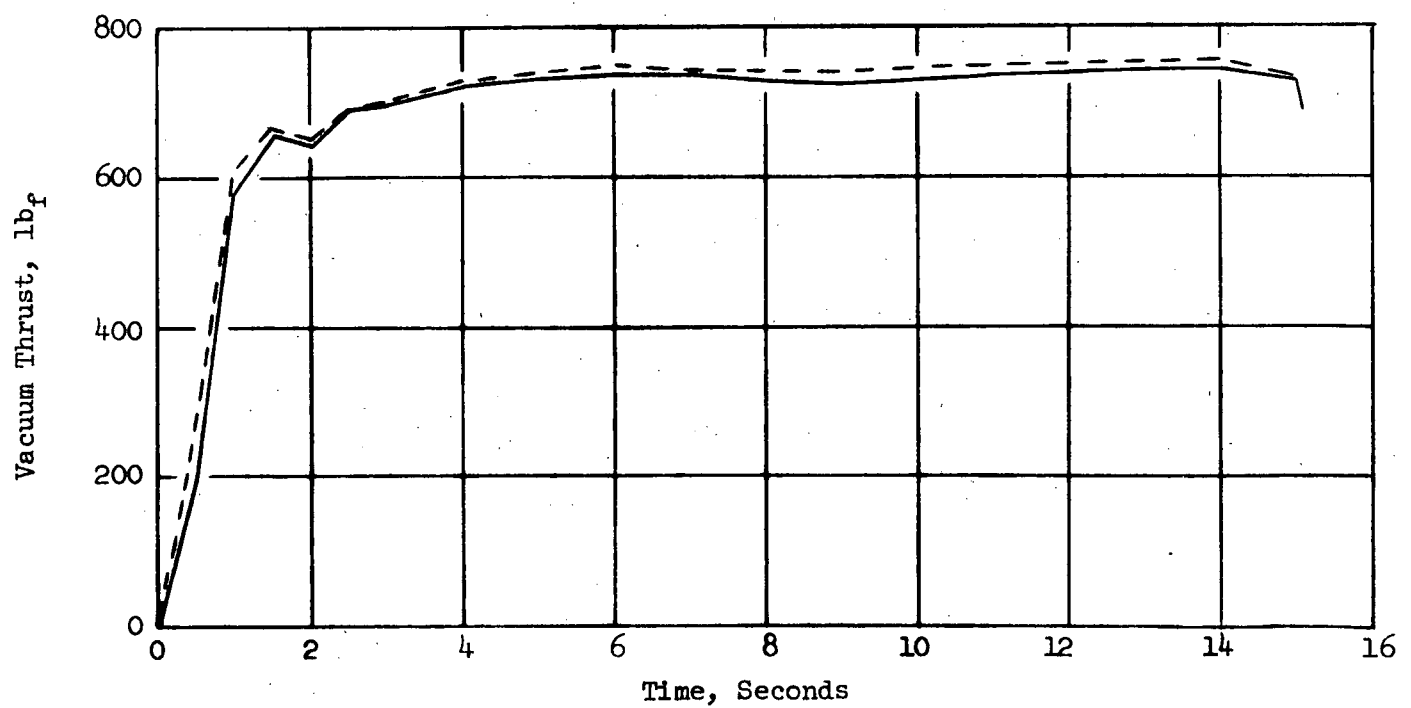
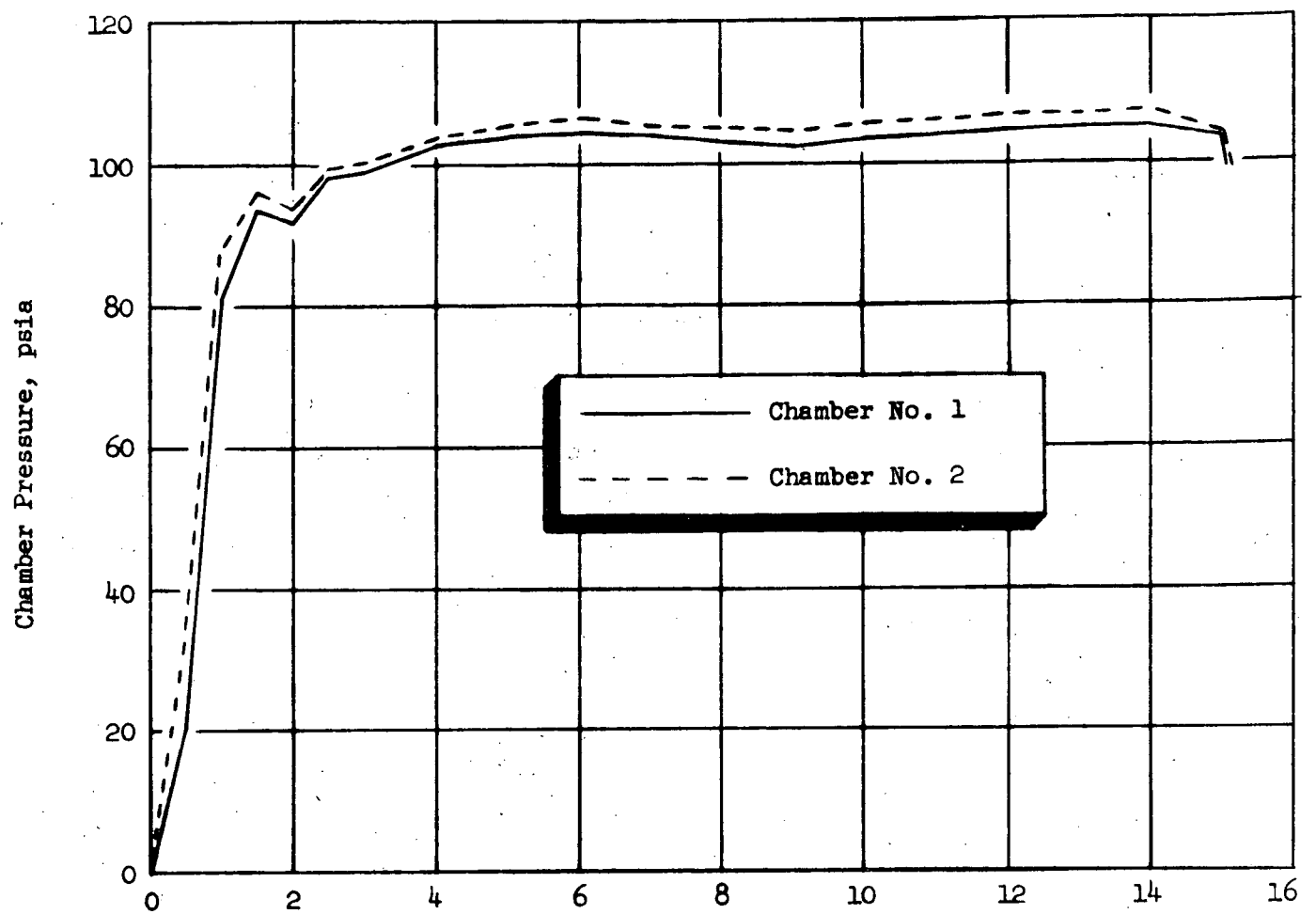
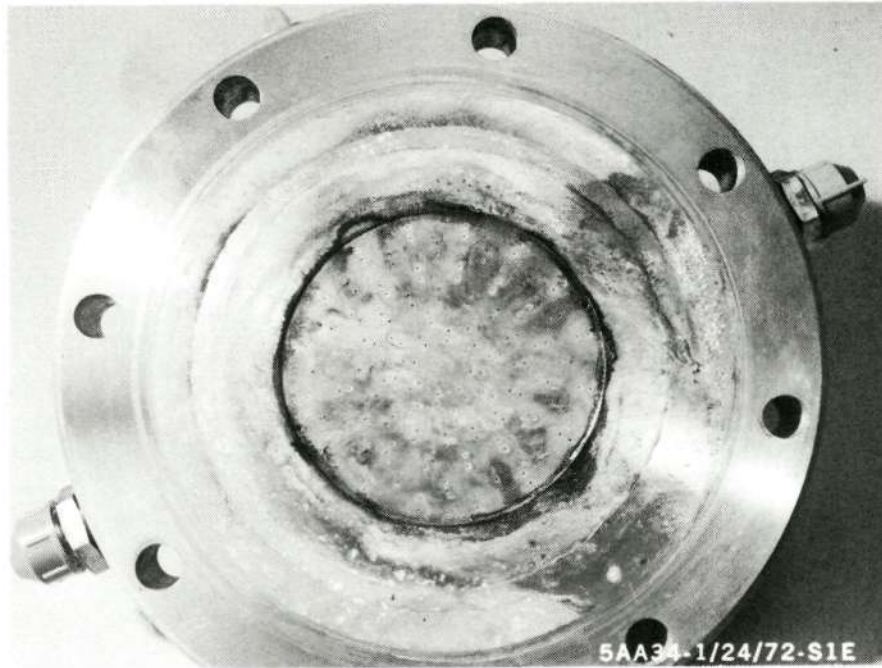


Figure 41. Chamber Pressure and Thrust for the Two Acceptance Tests

Figures 42 through 44 illustrate the post-test condition of the thrust chamber components. Some discoloration is evident in the chamber liner and throat insert; however, there was no measurable erosion in these areas. Pretest and posttest throat diameters were $2.540 \pm .001$ inch for both engines. There was no indication of ablative liner delamination or throat insert fractures in either of the two chambers.

Temperature responses at the back side of the graphite throat insert are presented in Fig. 45. All of the other thermocouples, located in the ablative materials, did not indicate any measurable temperature rise during the relatively short firings. The temperature at the start of convergence initially rises more rapidly than at the throat. This is due to the difference in thickness of the graphite insert at these locations. The throat would eventually become hotter as the temperatures approach steady-state. During the F_2/N_2H_4 demonstration firing, the crossover occurred at about 140 seconds.



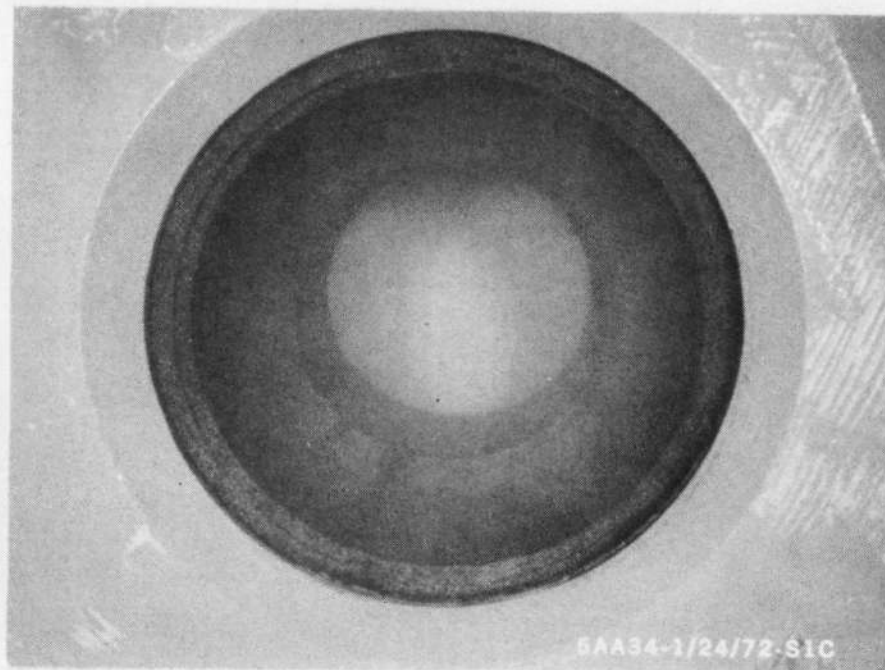
R.E.A. No. 2

Reproduced from
best available copy.

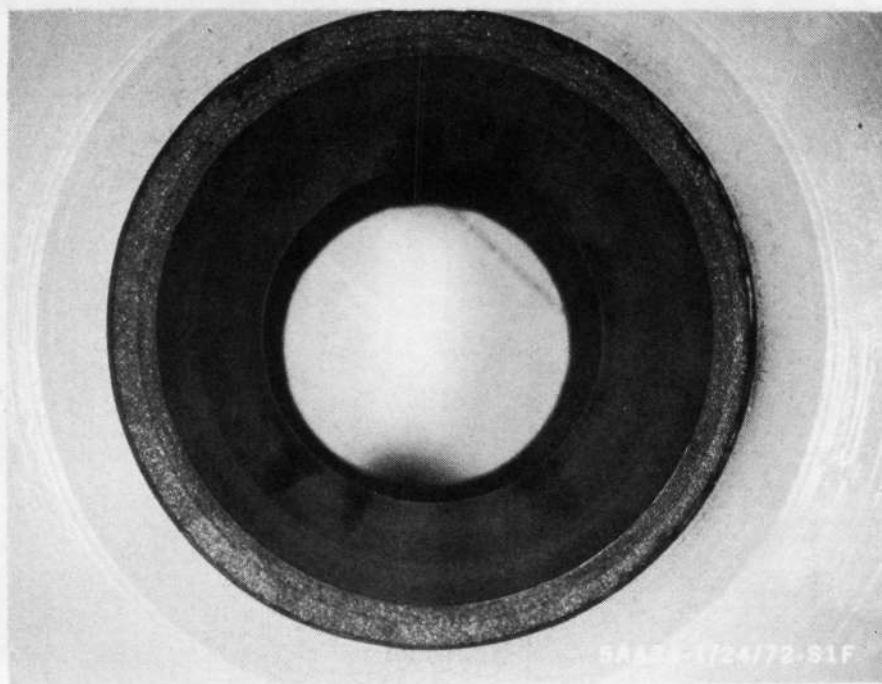


R.E.A. No. 1

Figure 42. R.E.A. Like-Doublet Injectors After 15-Second Acceptance Tests

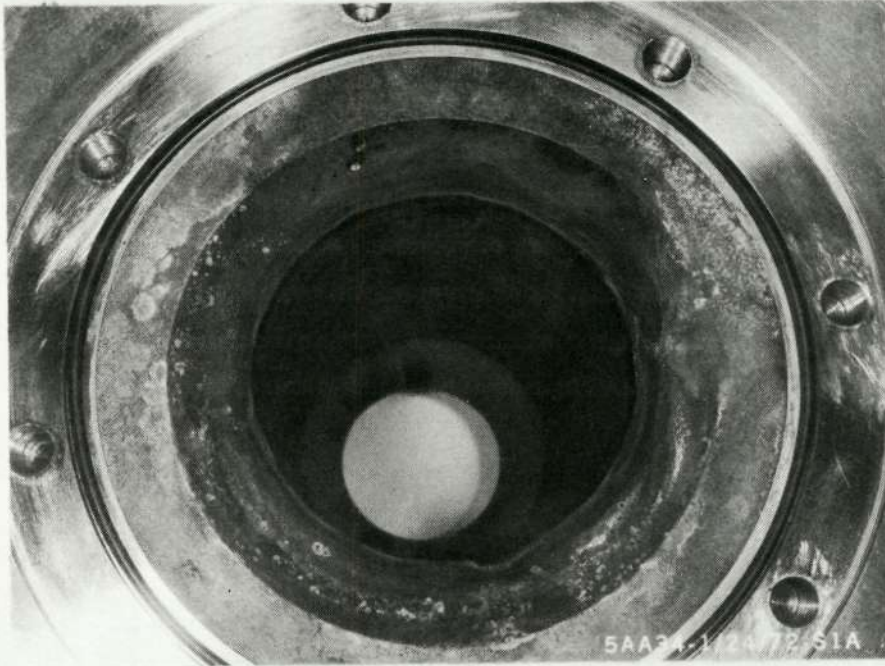


R.E.A. No. 2



R.E.A. No. 1

Figure 43. R.E.A. Graphite Throat Insert After 15-Second Acceptance Test



R.E.A. No. 2

Reproduced from
best available copy.



R.E.A. No. 1

Figure 44. R.E.A. Ablative Liner After 15-Second Acceptance Test

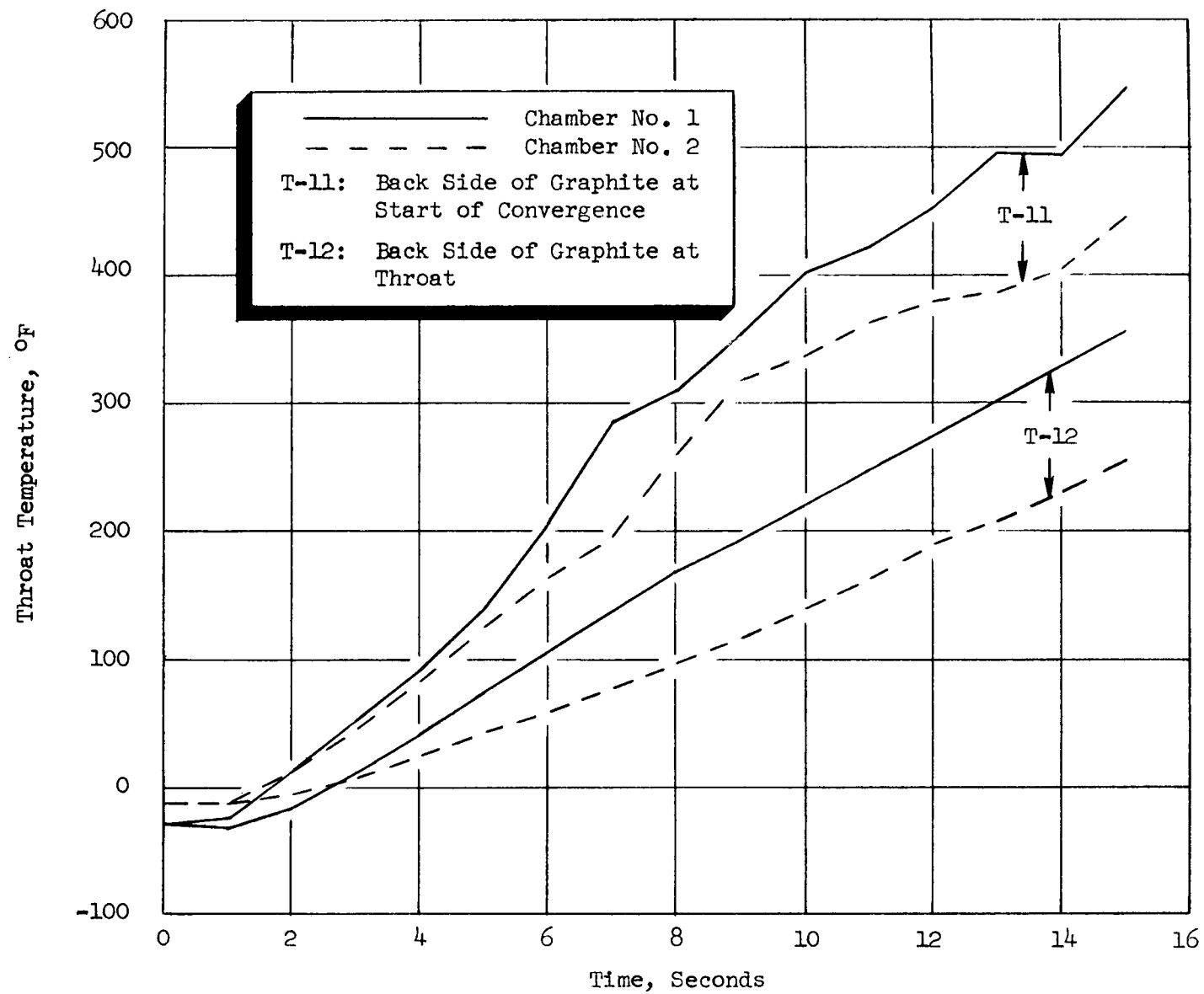


Figure 45. Throat Temperature Response Measured During the Two Acceptance Tests

CONCLUDING REMARKS

The overall objectives of the program were accomplished. The REA acceptance tests successfully demonstrated component durability and high performance. Also, the technique of electrical discharge machining, as opposed to conventional drilling, was found to be the superior method in the manufacture of small-orifice nickel injectors. This resulted in the attainment of more consistent overall discharge coefficients between injectors.

The feasibility of using the F_2/N_2H_4 propellant combination with the FLOX/MMH hardware was successfully demonstrated. Some minor problems were uncovered: (1) the relatively high head-end erosion of the ablative liner, (2) the freezing of the N_2H_4 in fuel manifold, and (3) the suspected N_2H_4 -nickel reaction after the 500-second demonstration test.

REFERENCES

1. R-6028-2, "Chamber Technology for Space Storable Propellants - Task II," Rocketdyne, a Division of North American Rockwell Corporation, Canoga Park, California, October 1965.
2. R-6561-2, "Chamber Technology for Space Storable Propellants," Rocketdyne, a Division of North American Rockwell Corporation, Canoga Park, California, September 1966.
3. Rupe, J.H., "Experimental Correlation of the Nonreactive Properties of Injection Schemes and Combustion Effects in a Liquid Propellant Rocket Engine", Tech. Report No. 32-225, JPL, July 1965.
4. Bartz, D. R., "A Simple Equation for Rapid Estimation of Rocket Nozzle Heat Transfer Coefficients," Jet Propulsion Laboratory, January 1957.